Geomorphology 485 (2025) 109859

Contents lists available at ScienceDirect

Geomorphology

journal homepage: www.journals.elsevier.com/geomorphology

Surface karst geomorphology in the Jahani salt extrusion, Zagros Mountains, Iran

Francisco Gutiérrez [a,*], Issa Ilyati [b], Mehdi Zarei [b]

[a] Department of Earth Sciences, University of Zaragoza, Spain
[b] Department of Earth Sciences, Shiraz University, Iran

ARTICLE INFO

Keywords:
Sinkhole
Polygonal karst
Polje
Salt escarpment
Salt rimstone
Salt glacier

ABSTRACT

This work analyses the superlative salt karst developed on Jahani salt extrusion (ca. 70 km^2, 900 m in local relief). This active diapir is expressed as a salt fountain comprising a summit dome above the feeding vent and laterally spreading salt glaciers (i.e., namakiers) moving at rates of the order of cm/yr. The salt extrusion hosts the first documented and mapped salt karst poljes, developed at the foot of the steep rock salt slopes of the summit dome by differential suballuvial dissolution and expansion by rim dissolution. A cartographic inventory of 6489 sinkholes has allowed to characterise morphometrically the differences between the juvenile and mature sinkhole landscapes developed in the proximal and distal sectors of a namakier, respectively. Sinkholes developed in the recently expelled salt at the proximal sector have an average length four times smaller (23 m versus 83 m) and a density three times higher (600 versus 200 sinkholes/km^2), reflecting the variable impact of expansion and coalescence processes. The Firuzabad River has trimmed the northern namakier, generating a 6 km long and > 400 m high salt escarpment, likely the largest on Earth. The dynamics of the escarpment is governed by the antagonistic roles of salt flow and rapid erosion by fluvial undermining, rock falls and dissolutional removal of the rock salt debris, causing severe hydrochemical degradation of the river waters. Exceptional halite rimstones occur in a marginal stream largely fed by permanent brine springs.

1. Introduction

Rock salt in active diapirs is a very special karst bedrock, not only because of its extremely high solubility (356 g/l), but also because of its mobility. Salt, due to its negligible yield strength, especially when wet, can experience viscous strain under very low differential stress and at surface temperature conditions. Salt flow can be driven by two mechanisms that may operate in combination; buoyancy related to density inversion of buried salt, and more importantly, differential loading (Hudec and Jackson, 2007). Differential loading can be induced by lateral tectonic forces (compression, extension) and vertical gravitational load. Flowing salt can rise towards the surface deforming the overlying and surrounding sediments, and generating salt structures with a discordant contact with the enclosing rocks (i.e., salt diapirs). Eventually, salt diapirs may emerge at the surface, generating salt extrusions in which exceptional karst landscapes can develop.

The most remarkable examples of salt extrusions are the emergent diapirs of Hormuz salt (late Neoproterozoic-early Cambrian) of the Fars Arc in the Zagros Mountains of Iran (Hudec and Jackson, 2007). These diapirs are widely regarded as old salt structures with long-sustain activity during the pre-shortening sedimentation phases, that have experienced rejuvenation by tectonic loading (i.e., squeezing) during the ongoing Cenozoic collision (e.g., Jahani et al., 2009, 2017). These salt extrusions display different morphological evolutionary stages (Jahani et al., 2007; Talbot and Pohjola, 2009; De Waele and Gutiérrez, 2022). Initially, the salt spelled from the vent forms a growing dome. When the weight in the dome exceeds the yield strength of the salt, it spreads laterally to form a salt fountain with a summit dome and salt glaciers, designated as namakiers (Talbot and Jarvis, 1984a, 1984b) (*namak* means salt in Farsi). Salt fountains in the Zagros can reach >10 km in length, may reach a local relief of 1.5 km, and typically move at rates of the order of cm/yr (see review in Pérez-Villar et al., 2025). When the salt supply ceases, the summit dome experiences deflation and the namakiers become stagnant, to form a salt droplet. Degrading salt domes and salt droplets experience progressive wasting (i.e., retreat and deflation) by dissolution and mechanical erosion, ultimately leading to the formation of flat-floored craters underlain by detrital deposits and dissolution residues.

* Corresponding author.
E-mail address: fgutier@unizar.es (F. Gutiérrez).

https://doi.org/10.1016/j.geomorph.2025.109859
Received 25 April 2025; Received in revised form 26 May 2025; Accepted 26 May 2025
Available online 29 May 2025

Williams (2011), in his work on the representation of karst landscapes in the UNESCO World Heritage List, reports that numerous sites include karst features with outstanding universal value (i.e., the best of the best), or international significance. However, he identifies as major gaps in coverage: karst regions such as the Middle East, karst arid and semiarid karst environments, and especially, evaporite karsts. Supported by these gaps and considering the superlative value of the salt extrusions of the Zagros, he suggested that a selected group of sites that illustrate the evolution of emerged salt diapirs and their landforms could make an excellent World Heritage nomination. The salt diapirs of the Fars Arc have been the focus of a number of studies dealing with various topics, such as the interaction with the associated tectonic structures (Talbot and Alavi, 1996; Jahani et al., 2009, 2017; Gutiérrez et al., 2024), internal structure and mechanics of salt flow (Talbot, 1979; Talbot and Jarvis, 1984a, 1984b; Talbot and Pohjola, 2009), long-term rates of uplift based on geochronological data (Bruthans et al., 2010), DInSAR and geodetic measurements of surface displacement (Talbot et al., 2000; Aftabi et al., 2010; Ghassemi and Roustaei, 2021; Zhang et al., 2021; Shami et al., 2024), surface and subsurface hydrology (Zarei and Raeisi, 2010; Bruthans et al., 2017), erosion rates (Bruthans et al., 2008), caves (Bosák et al., 1999; Bruthans et al., 2024), hydrochemical degradation of adjacent water resources (Zarei, 2016 and references therein). However, studies thoroughly addressing the surface karst geomorphology of the salt extrusions are almost lacking, with the exception of the work by Zarei and Raeisi (2010) in the Konarsiah diapir.

This work analyses the surface karst geomorphology of Jahani salt fountain (Jahani means salt mountain of the universe; Abirifard et al., 2017). Jahani salt extrusion stands out for its superlative scenery and exceptional geomorphic diversity, constituting an excellent candidate for a World Heritage Nomination. The main issues address in this work include: (1) the morphometric features in a polygonal landscape of tightly packed sinkholes showing morpho-chronological gradation for the proximal to the distal sectors of the salt glaciers; (2) the first documented salt karst poljes; (3) an extraordinary salt escarpment 6 km long and >400 m high, which is probably the largest on earth; (4) exceptionally large and aesthetically valuable halite rimstones; and (5) highly dynamic fluviokarst landscape.

2. General features of the Jahani salt extrusion and previous work

2.1. Geological setting

The Jahani salt extrusion is located in the NW-SE trending Zagros Fold-and-Thrust Belt, related to the oblique NNE-directed convergence between the Arabian and Eurasian tectonic plates (Vernant et al., 2004; Walpersdorf et al., 2006) (Fig. 1A). More specifically, Jahani Diapir occurs in the Fars Arc of the Simply Folded Belt of the Zagros; outer sector of the orogenic wedge (Fig. 1B). The Fars Arc is an arcuate belt of folds detached along the Hormuz salt (Jahani et al., 2009). This late Neoproterozoic-early Cambrian salt formation, with an initial thickness of around 1–1.5 km, was deposited in extensional basins controlled by N-oriented faults (Kent, 1979; Talbot and Alavi, 1996; Jahani et al., 2017). The mechanically weak Homuz salt decouples the cover from the more rigid basement and forms more than one hundred emergent or buried diapirs (Fig. 1B) that penetrate through a 12–15 km thick sedimentary overburden (Kent, 1958, 1979; Jahani et al., 2009, 2017; Gutiérrez et al., 2023b). These are widely regarded as precursor diapirs, initially developed in pre-orogenic times (Harrison, 1930; Kent, 1979; Talbot and Jarvis, 1984a, 1984b; Talbot and Alavi, 1996; Sherkati et al., 2006; Jahani et al., 2007, 2009, 2017; Snidero et al., 2019), that have experienced rejuvenation by contractional loading (i.e., squeezing) during the Cenozoic collision (Jahani et al., 2007, 2017; Gutiérrez et al., 2023b). The deformation in the Fars Arc has propagated progressively to the SW since the Eocene-Oligocene transition (Hessami et al., 2001a). Nonetheless, the initiation of substantial morphogenetic folding and relief development in each sector of the folded foreland is recorded by the basal unconformity of the conglomeratic Plio-Quaternary Bakhtyari Formation, progressively younger towards the SW (Hessami et al., 2001a; Mouthereau et al., 2007; Ruh et al., 2014; Gutiérrez et al., 2023a, 2023b).

In the western Fars Arc, the majority of the salt extrusions occur associated with N- to NNW-trending right-lateral strike-slip faults, including from W to E the Kazerun-Borazjan, the Kareh-Bas (or Mengarak) and the Sarvestan fault systems (Berberian, 1995; Authemayou

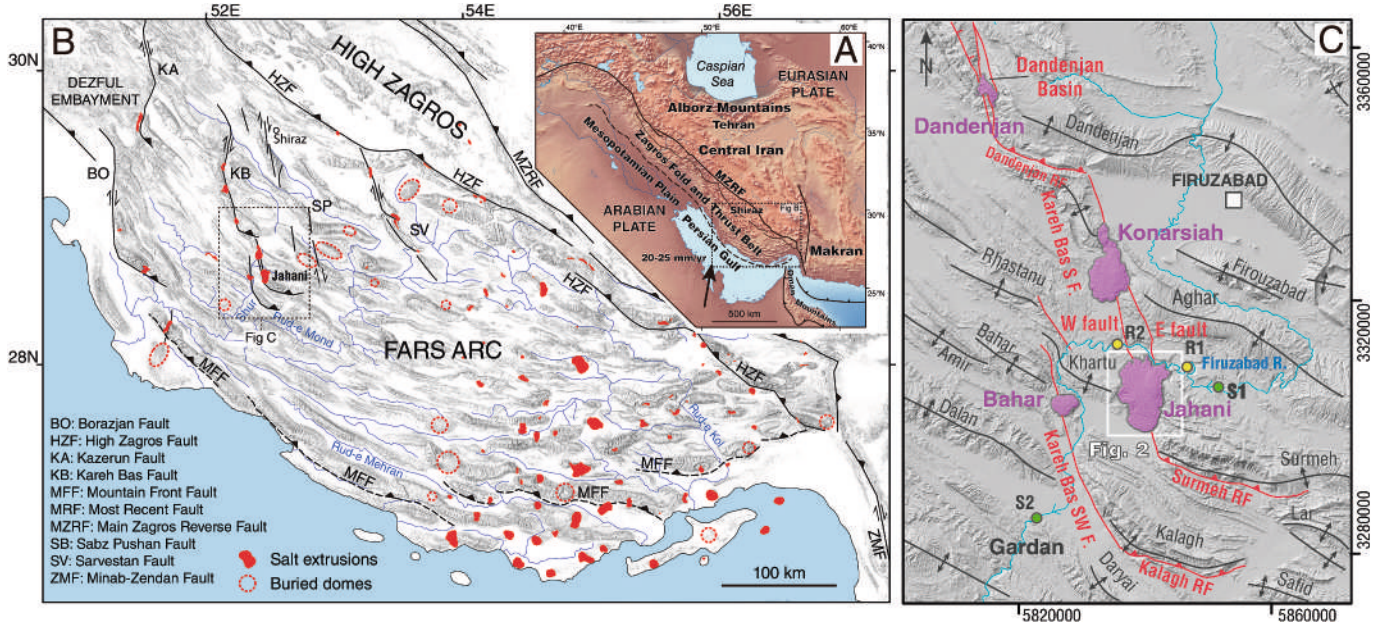

Fig. 1. General setting of the Jahani salt extrusion. A: Geotectonic setting of the Zagros Fold-and-Thrust Belt related to the ongoing oblique convergence between the Arabian and Eurasian plates. Vector displacement of the Arabian Plate from GPS data published by Vernant et al. (2004). B: Hillshade of the Fars Arc in the Simply Folded Belt showing the diapirs of Hormuz salt (emergent and buried) and the main faults. C: Shaded relief model with the southern section of the Kareh Bas fault system and the associated salt extrusions. Circles (Rx and Sx) indicate the location of stations in the Firuzabad (or Shur) River used to assess variations in dissolved salt.

et al., 2006; Jahani et al., 2017; Hassanpour et al., 2018; Gutiérrez et al., 2024; Gutiérrez et al., 2025b) (Fig. 1B). These faults, nearly parallel to the plate convergence vector, display the following features (Berberian, 1995; Hessami et al., 2001b; Bachmanov et al., 2004; Authemayou et al., 2006, 2009; Tavakoli et al., 2008; Faghih et al., 2016; Hassanpour et al., 2018; Gutiérrez et al., 2024; Gutiérrez et al., 2025b; Nezamzadeh et al., 2024; Authemayou et al., 2009) (Fig. 1C): (1) right-lateral offset of folds and local deflection of fold axes; (2) alignments of salt extrusions; (3) several geometric segments, often terminating at their southern end with reverse-fault eastward bends associated with the steeper or overturned southern limb of anticlines; and (4) evidence of Quaternary deformation and ascribable damaging earthquakes. These orogen-oblique dextral faults have been interpreted as tear faults that accommodate more rapid translation of the cover above thicker salt (i.e., lower basal friction), associated with the hanging wall of down-to-the-east basement faults that controlled sedimentation in Hormuz times. The development of these supra-salt faults was also promoted by rows of pre-collision salt walls and stocks overlain by thin overburden (Jahani et al., 2017; Hassanpour et al., 2018; Gutiérrez et al., 2024, 2025b).

The Jahani salt extrusion is associated with the NNW-SSE-oriented and 56 km long southern segment of Kareh Bas Fault, which southern termination corresponds to the Surmeh reverse fault along the southern limb of the SSW verging Surmeh Anticline (Gutiérrez et al., 2024, Gutiérrez et al., 2025b) (Fig. 1C). GPS measurements carried out with a dedicated network indicate a horizontal slip rate of 3.4 ± 0.3 mm/yr across the Kareh Bas fault system (Tavakoli et al., 2008). Jahani is the southernmost salt extrusion of a row of five emergent diapirs located along the Kareh Bas N and S fault segments (Fig. 1B). These salt extrusions show a morphological gradation, ranging from the three degraded salt extrusions in the north, to the Kornarsiah salt fountain transitioning to a salt droplet (Zarei et al., 2012), and Jahani, a vigorously rising salt fountain with a well-defined summit dome (Abirifard et al., 2017; Gutiérrez et al., 2025b) (Fig. 1C). This gradation is likely related to the N-to-S successive emergence of salt diapirs associated with the southward propagation of the Kareh Bas fault system and the creation of new structural discontinuities for salt breakout from precursor diapirs at contracting anticlines (Gutiérrez et al., 2024).

The geology around the Jahani salt extrusion is described in Gutiérrez et al. (2025b). The geological structure in the study area is characterised by NW-SE to WNW-ESE trending folds offset by the right-lateral Kareh Bas strike-slip fault (Talbot and Alavi, 1996; Jahani et al., 2017; Hassanpour et al., 2018). Here, the southern segment of the Kareh Bas fault comprises two strands with a right-stepping arrangement, designated as the western and eastern faults (labelled W and E fault in Fig. 1C). The releasing stepover overlaps between the Konarsiah and Jahani salt extrusions. The latter occurs associated with the northern termination of the western fault and the southern termination of the eastern fault, respectively. The eastern fault strand offsets dextrally 4.5–5 km the axis of the Aghar Anticline. The western fault strand offsets right-laterally 5–5.5 km the axis of the Khartu-Surmeh Anticline. Between the Aghar Anticline and the Surmeh Anticline there is broad synclinorium (GSI, 1996) with a secondary open anticline (Shur Anticline), which axis roughly coincides with the path of the Firuzabad (or Shur) River. The eastern (and northern) strand of the Kareh Bas Fault likely propagated southwards and stepped over a precursor buried Jahani Diapir (or Konarsiah Diapir), initiating the development of the western (and southern) strand (Gutiérrez et al., 2025b). Weak zones such as diapirs typically promote the development of stepovers and fault segmentation (Mann et al., 1983; Dooley and Schreurs, 2012). The pulling apart of the thin overburden above the precursor Jahani Diapir, now located at a releasing stepover, eventually created the opening through which the salt has emerged. A similar strike-slip fault and diapir interaction-evolution has been proposed for the Dandenjan Diapir and the associated Dandenjan pull-apart basin to the north (Gutiérrez et al., 2024) (Fig. 1C). The western fault strand has deformed a late Pleistocene terrace of the Firuzabad River lying at 40 m above the current channel (39R 640463E 3,171,919 N). Here, stratigraphic and structural relationships together OSL ages allowed to infer a minimum of two paleoearthquakes accompanied by surface deformation events occurred during the accumulation of the terrace deposit. The most recent event occurred at 14.7–13.8 ka (Gutiérrez et al., 2025b). The numerical ages obtained from the +40 m terrace deposit indicate a long-term incision rate of 2.7–2.9 mm/yr (Gutiérrez et al., 2025b), consistent with the downcutting rates estimated by Oveisi et al. (2009) in the same region.

The Hormuz Group extruded at Jahani displays intercalations of non-evaporitic reddish rocks with an overall concentric distribution (Kent, 1958; Talbot and Alavi, 1996; Talbot et al., 2000; Tayebi et al., 2013) (Fig. 2). The outermost intercalation is a laterally continuous ridge-forming unit, consisting of red limestones and marls with a conformable breccia of black dolostone veined with sphalerite. Talbot and Alavi (1996) and Talbot et al. (2000) proposed that this overturned unit of putative Cambrian age separates the Hormuz Group into two successions: (1) an inner older succession (Neoproterozoic component) of thick bedded multi-coloured halite interbedded with anhydrite, dark foetid dolomites and other subordinate lithologies (sandstones, siltstones, marls, orthoquartzites); and (2) a younger succession (Cambrian component) in the outer fringe of the salt fountain dominated by grey and bluff halite with dispersed anhydrite and volcanic inclusions. The distribution of the units, with an overall recumbent fold structure, suggests that the younger salt unit (Cambrian?) extruded first and was overturned and overridden by the older unit (Neoproterozoic?), with some potential decoupling between the salt units and the more competent intervening non-evaporitic bed. A mineralogical analysis of a rock salt sample from Jahani carried out by Bruthans et al. (2009) indicated 93.1 % halite, 4.7 % silicates and oxides, and < 2.1 % gypsum and anhydrite.

2.2. General geomorphological features

The Jahani salt fountain is 12.35 km long and 7.37 km wide, covers 67.9 km^2 and has a local relief of 918 m between highest point of the summit dome and the lowest point of the southern namakier front (Fig. 2). Gutiérrez et al. (2025b) roughly estimated a volume of 8500 Mm^3 for the extrusion computing the 3D space enclosed by the topography of the salt fountain and a basal surface interpolated from its perimeter, plus applying a correction factor of 0.8 to account for the general elevation rise of the base of the salt glaciers towards the opening of the vent. Both the salt fountain and the summit dome display a N-S elongated geometry parallel to the Kareh Bas Fault (Fig. 1C). The summit dome (red dashed line in Fig. 2), 5 km long and 2.5 km wide, covers 9.4 km^2 (ca. 14 % of the salt fountain) and stands proud around 250 m above the proximal sector of the surrounding namakiers. The eccentric position of the summit dome on the NE sector of the salt extrusion reflects the position of the elongated pull-apart vent through which the salt is expelled under a transtensional regime. The extruded salt spreads radially from the summit dome towards topographically lower ground, forming salt glaciers with frontal lobes laterally confined by ridges in the countryrock (Fig. 2). The northern namakier, which cascades towards the deeply entrenched Firuzabad (or Shur) River valley, is trimmed by fluvial erosion showing a large salt escarpment. Here, the salt extrusion descends as much as 500 m in a distance of around 1 km (27° slope). The southern lobe, 5.4 km long and 5.2 km wide, overrides an alluvial piedmont and its eastern flank is over-steepened by fluvial undermining related to a lateral drainage. On the western sector, SW- and NW-directed lobes 3.2 and 4.8 km wide, respectively, have advanced through erosional gaps. The west- and south-flowing namakiers (i.e., salt glaciers), unaffected by erosion along their distal sector, have general slopes within the range of 6.6–7.5°.

The salt exposures mapped in this work cover 6.93 km^2, representing 10.2 % of the extrusion (11 % in Abirifard et al., 2017 and Bruthans et al., 2024) (Fig. 2). They occur on steep slopes where rapid erosion overwhelms the production of residual soils by dissolution: escarpment

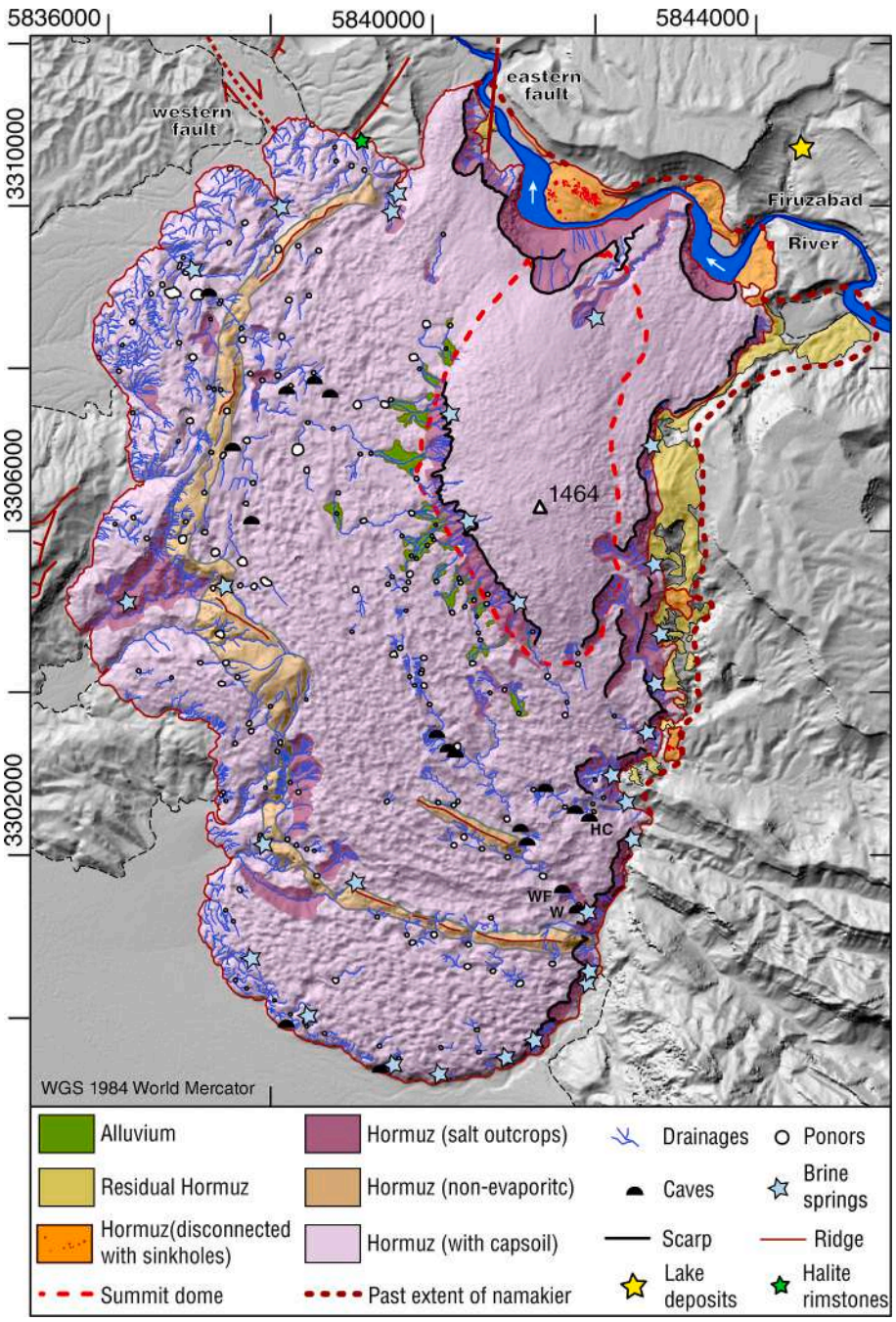

Fig. 2. Geomorphological map of Jahani salt extrusion indicating the maximum extent reached by the salt fountain in the past, eventually damming the Firuzabad River and creating a lake upstream. The yellow star indicate lake deposits OSL-dated by Gutiérrez et al. (2025b) at 28 ± 5 ka. Ponors indicate swallow holes that absorb water from gully networks. The location of brine springs and caves is based on Bruthans et al. (2024) and Abirifard et al. (2017), respectively.

of the Firuzabad River, steep flanks of the summit dome, eastern side of the southern namakier, deeply entrenched gullies (western lobes), and steep slopes in karst depressions. The rest of the salt extrusion is underlain by soils resulting from dissolution of the salt bedrock and the in situ accumulation of the residue (i.e., capsoils). This regolith consists of massive and hardened fine-grained material with floating or clast-supported gravel- and boulder-sized clasts of multiple lithologies. The clasts may correspond to inclusions formerly embedded within the salt, or breccias derived from non-evaporitic beds intercalated within the Hormuz series. The capsoil often diplays a thin crust related to secondary gypsum precipitation (Bruthans et al., 2009; Zarei et al., 2012). Most of the summit dome is underlain by capsoil of decimetre- to metre-scale thickness, while the salt glaciers display a more indurated capsoil meters or tens of meters thick with sparse vegetation (Bruthans et al., 2009; Abirifard et al., 2017). Note that the development of a capsoil 10 m thick from rock salt with 90 % purity requires the dissolution of at least 100 m of salt bedrock. Bruthans et al. (2009) characterised the mineralogical composition of thick capsoils in the namakiers of Jahani based on 9 samples, obtaining the following average values: silicates and oxides (38.9 %), carbonates (30.5 %), gypsum/anhydrite (27.8 %), halite (2.8 %). They found that gypsum and halite content increases with depth, suggesting that these soluble minerals are leached by percolating water close to the surface. An analysis of soil water indicated a total dissolved solids (TDS) content of 0.15 g/l and Ca-HCO3 hydrochemical facies (Bruthans et al., 2017). Additionally, the results of 11 infiltration tests carried out in thick capsoils, with a mean value of 315 mm/h,

indicated low runoff coefficients. Nonetheless, a significant proportion of the soil water is lost by evaporation or plant transpiration. Bruthans et al. (2008) measured erosion over a period of 5 years (2000–2005, rainfall total 1474 mm) in Jahani using plastic pegs 11 cm long placed on exposed rock salt (14 pegs in rillenkarren and gullies) and capsoils (4 pegs), but a considerable proportion of the pins were wash away. The obtained vertical denudation rates per 100 mm rainfall in the pegs that remained in rock salt ranged between 9 and 28 mm for the period 2000–2024 and from 15 to 51 mm for the interval 2004–2005. Bruthans et al. (2008) observed that erosion rates are inversely proportional to inclination; the greater the gradient, the larger the surface exposed to vertical rainfall.

Abirifard et al. (2017) reported a polygonal karst landscape of densely packed sinkholes <10 m across in the summit dome. They also constructed an incomplete cartographic inventory of 3590 sinkholes >10 m long in the namakiers covering 10.5 % of the area and estimated a density of 73 sinkholes/km^2. The largest sinkholes were found in the distal sector of the salt glaciers, reaching a maximum length of 459 m. Bruthans et al. (2024) documented 18 explored caves in the namakiers of Jahani with a total length of 3.5 km. They differentiated two types of caves: (1) shafts with short subhorizontal channels at their bottom (inlet caves); and (2) high-gradient (11–19 %) and sinuous vadose canyons with steps in the longitudinal profile that extend from an inlet, commonly associated with a blind valley, to an outlet (integrated caves). The depth distribution of caves and shafts indicates that rock salt can be permeable to depths of around 70–100 m. The longest integrated caves, located in the eastern sector of the southern namakier, are White Foam (1262 m long), Hidden Creek (478 m), and Waterfall (424 m) (labelled as WF, HC and W in Fig. 2, respectively). Based on the distribution of detrital deposits within these integrated caves and 12 radiocarbon ages from wood fragments found within the clastic deposits, perched up to 11.3 m above the cave floor, they constrained the age of the caves, reconstructed their rapid evolution and calculated incision rates. The data revealed that the caves formed over the last ca. 600 years, and allowed calculating incision rates of 3–11 cm/yr in White Foam and Waterfall caves and 2–7 cm/yr in Hidden Creek cave. These rates should be considered as minimum values based on a maximum age for the incision period because of the following reasons: (1) the age of deposition is younger than the age of the death of the plant; (2) incision started sometime after accumulation of the wood fragment; and (3) the wood fragment may have been reworked from older deposits. Additionally, they inferred a period in which cave evolution was dominated by detrital filling accompanied by upward paragenetic incision (i.e., antigravitative erosion). Factors such as blocking of caves by major earthquakes and high erosion rates related to overgrazing and/or climate change were proposed as potential drivers for this anomalous speleogenetic trend (Bruthans et al., 2024).

2.3. Hydrology and hydrochemistry

Mean annual precipitation at Firuzabad meteorological station, located 23 km to the north and at 1330 m a.s.l., is 408 mm (1988–2010; Naderi et al., 2016). The rainy season spans between November and April, typically with 15–30 rainy days per year and frequent severe storms (Bruthans et al., 2017). The average temperature ranges from 20 to 25 °C, and potential annual evapotranspiration is around 2800 mm. The area with external drainage, associated with the salt escarpment and steep and deeply dissected catchments at the margins of the salt glaciers, has been estimated in this work at 12.7 km^2 (18.75 %). Abirifard et al. (2017) documented 26 permanent brine springs and 4 temporary brine springs, the latter associated with the summit dome, all of them saturated with respect to halite (Fig. 2). The perennial brine springs are

Fig. 3. Salt exposures in the eastern flank of the southern namakier dissected by a dense gully network. Here, the flank of the salt glacier in undermined and oversteepened by a marginal stream. PBS: Perched brine spring, CS: Discontinuous capsoil, C: Colluvium made up of reworked dissolution residues.

mostly perched above the surrounding ground, marking the base level of the karstified permeable bedrock (Fig. 3). The perched nature of these springs is largely related to rapid slope retreat (eastern flank of the southern namakier) or fluvial incision. The average TDS of the brine springs is 317 g/l, the share of dissolved sodium chloride 98 %, and the total average discharge 32 l/s. Based on these figures, Bruthans et al. (2024) estimate that around 320,000 tons of dissolved halite (ca. 150,000 m^3, halite density 2.17 g/l) are released annually from the salt extrusion via brine springs. In addition, a considerable amount of dissolved salt may also be transferred through subsurface brine flows into the adjacent alluvial and karst aquifers (Mehdizadeh et al., 2015; Zarei, 2016; Abirifard et al., 2017). To the west of the salt extrusion, Abirifard et al. (2017) identified two brackish springs in a carbonate aquifer intruded by brine from the diapir, with an estimated contribution of around 2 l/s. The dissolved salt may originate from chemical denudation in salt exposures, subsoil dissolution at the rockhead, and karstification within the permeable zone of the salt bedrock. The annual volume of precipitation recharging at Jahani salt extrusion can be roughly estimated at 2 MCM/yr considering an annual rainfall of 408 mm, an area of 54.4 km^2 with internal drainage (81.3 %), and the recharge coefficient of 9 % estimated in the Konarsiah diapir (Zarei et al., 2012), while the annual volume of brine released from the springs can be estimated at 1 MCM/yr considering an average total flow rate of 34 l/s. This confirms subsurface drainage of the diapir into the neighbouring aquifers. Tritium activity at brine springs indicate that modern recharge (post-1950) dominate the base flow, indicating limited residence time, largely regulated by capsoils (Bruthans et al., 2017).

Bruthans et al. (2017) documented a storm-related flash flood event at Jahani (30 March 2009; 64 mm rainfall). Flood water caused the temporary flooding of some sinkholes and blind valleys and total infiltration was achieved within two days. They estimated that 6–10 % of the rainfall generated rapid runoff, while 90–94 % infiltrated in capsoils, most of which was subsequently evaporated. Interestingly, TDS in the water at brine springs during the flood were substantially and slightly undersaturated with respect to halite. Naderi et al. (2016), using discharge and hydrochemical data from two distant stations in the Firuzabad River (labelled as S1 and S2 in Fig. 1), estimated the contribution of Konarsiah, Jahani and Bahar (or Khurab) diapirs to the increase in dissolved solids in the river and its hydrochemical degradation. In the upstream station, with an average discharge of 5 m^3/s, the mean TDS is 492 mg/l and the dominant hydrochemical facies is calcium or magnesium bicarbonate. In contrast, in the downstream station, with a mean flow rate of 9.8 m^3/s, the average TDS is 7075 mg/l (ca. 14 times higher) and the hydrochemical facies of the water is permanently sodium chloride. These authors foresee greater degradation of the water in the near future related to the predicted decline in precipitation.

2.4. Long- and short-term dynamics

Gutiérrez et al. (2025b) mapped disconnected masses of salt-bearing Hormuz rocks with sinkholes and Hormuz-derived residual deposits along the northern and eastern margins of Jahani. These sediments, including portions of the northern namakier up to 120 m high that surmounted the northern margin of the Firuzabad valley, indicate that the salt extrusion reached greater extent in the past (dashed red line in Fig. 2) and dammed the Firuzabad River creating a lake 6–15 km long upstream. The OSL ages obtained from lake deposits situated upstream of the salt glacier dam (28 ± 5 ka) and from the faulted +40 m terrace of the Firuzabad River (ca. 14.7–13.8 ka), together with geometrical relationships (e.g., namakier dam inset with respect to +40 m terrace), indicate that the northern salt glacier of Jahani has dammed the Firuzabad River at least two times, at around 28 ka and sometime after 14–15 ka. In contrast, the frontal sector of the S-, SW- and NW-directed glacier lobes do not show any evidence of retreat. Gutiérrez et al. (2025b) also characterised the current kinematics of the Jahani salt fountain using decomposed vertical and horizontal (*E*-W) DInSAR displacement data, together with deformation time series. The deformation data reveal the following main patterns: (1) uplift in the southern sector of the summit dome at rates of around 1–2 cm/yr; (2) rapid subsidence (ca. -10 cm/yr) and lateral flow (ca. 15 cm/yr) in the northern sector of the summit dome where the salt is affected by erosional debuttressing; (3) lateral spreading at rates of ≤10 cm/yr in the steep flanks of the summit dome; (5) slow subsidence (ca. -1 cm/yr) around the well-defined junction between the summit dome and the W- and S-flowing namakiers; (6) lateral spreading of the namakiers unaffected by the debutressing effect of the salt escarpment at rates of 1–2 cm/yr; (7) slow uplift (<0.5 cm/yr) and probable horizontal displacement in the frontal sector of the NW and S lobes. Additionally, the displacement time series show continuous and rather constant creep deformation lacking any clear relationship with rainfall. These data, together with DInSAR studies carried out in other salt extrusion in the Zagros Mountains (see review in Pérez-Villar et al., 2025), challenge the erratic and inconsistent horizontal and vertical velocities of the order of m/yr measured by Talbot et al. (2000) and Zarei et al. (2012) in the Jahani and Konarsiah diapirs, respectively. Those geodetic measurements were obtained using inadequate markers (bushes, trees, blocks, cairns, salt pillars) and an insufficient number of theodolite stations, in some cases placed on mobile salt (Bruthans et al., 2024; Gutiérrez et al., 2025b).

3. Methodology

Preliminary geomorphological maps were elaborated through the interpretation under stereoscope of greyscale aerial photographs from December 1994 (National Cartographic Centre of Iran, approximate scale of 1:44,000). Field surveys were conducted in February 2012 and September 2023 using a tablet with georeferenced satellite images for navigation and location of observation and sampling points. The final geomorphological and sinkhole maps were produced with ArcMap using satellite images (ESRI World Imagery, Google Earth), TanDEM-X DEMs (12 m nominal resolution; German Aerospace Center, DLR), and various terrain models derived from the DEMs. The TanDEM-X DEM was used to compute a number of parameters for the morphometric characterisation of the salt extrusion and the karst depressions. These DEMs, derived from bistatic X-Band interferometric SAR data acquired by the satellites TanDEM-X (TDX) and TerraSAR-X (TSX), have absolute and relative vertical accuracies of <10 m and 2–4 cm, respectively. Elevations are defined with respect to the reflective surface of X-Band interferometric SAR returns. This implies, together with the sparse vegetation of the study area, that the used DEMs essentially represent Digital Surface Models (Wessel, 2016).

4. Results

4.1. Surface stream network

Great part of the Jahani salt extrusion displays a perfect holokarst landscape completely pockmarked by sinkholes and lacking any evidence of fluvial incision (Cvijić, 1893; De Waele and Gutiérrez, 2022). These include the upper part of the summit dome and extensive tracts in the low-gradient portions of the namakiers. The steep slopes on rock salt exposures are typically dissected by dense gully networks forming a badland-like landscape (Fig. 3). These gully systems may have an external drainage flowing into marginal streams (e.g., eastern flank of southern namakier) and the surrounding piedmonts, or feed the underground karst drainage typically through ponors (e.g., western flank of summit dome). Some areas with capsoil are also dissected by surface streams. The streams tend to form dense throughgoing networks in the steep slopes associated with the frontal sectors of the namakiers (NW lobe), locally extending into the non-evaporitic sediments intercalated within the Hormuz series. Some of these streams have been disrupted by collapse sinkholes functioning as ponors, separating a blind valley

upstream and a beheaded valley downstream (i.e., wind gap). In the low-gradient sectors of the salt glaciers the streams are mostly short and low order channels with limited forking that terminate at ponors. An exception is a long (3.7 km in straight length), discontinuous, SE-directed stream network in the southern glacier (Fig. 2).

4.2. Large alluviated depressions and poljes

A total of 19 large depressions with flat floors underlain by alluvium have been mapped (Figs. 2, 4, Table 1). Most of these depressions occur at the foot of the scarped western flank of the summit dome (i.e., proximal edge of namakier), and the majority of them are spatially associated with steep slopes on bare salt (Fig. 5). The alluvium covering the floor of the basins is a relatively well-sorted and polymictic gravelly deposit derived from the insoluble components of the Hormuz salt, either intercalated beds or inclusions. The main morphometric parameters of the depressions are indicated in Table 2, with a maximum area of 14.2 ha and a maximum axial length of 929 m. The depressions are dominantly elongated, with the major axes showing a radial pattern about the summit dome and consistent with the general slope. The floor of the depressions shows a dominant gradient away from the summit dome and the alluvial channels carved in the alluvium often terminate in ponors (Figs. 4 and 5). These swallow holes may correspond to cover collapse sinkholes developed on the alluvial surface, or to bedrock collapse sinkholes formed at the edge of the depressions.

Four main types of depressions can be differentiated on the basis of their morphology and hydrology (Table 1): (1) valley sections entrenched into the salt bedrock with flat alluviated floor; (2) relatively broad and scarcely entrenched alluvial aprons in the piedmont of the summit dome with throughgoing drainage; (3) semiclosed depressions with both throughgoing drainages and channels that flow into ponors; and (4) closed depressions with internal drainage via ponors and diffuse infiltration through the alluvial floor. The two former types are hydrologically open depressions. The latter two, including 14 depressions, fall

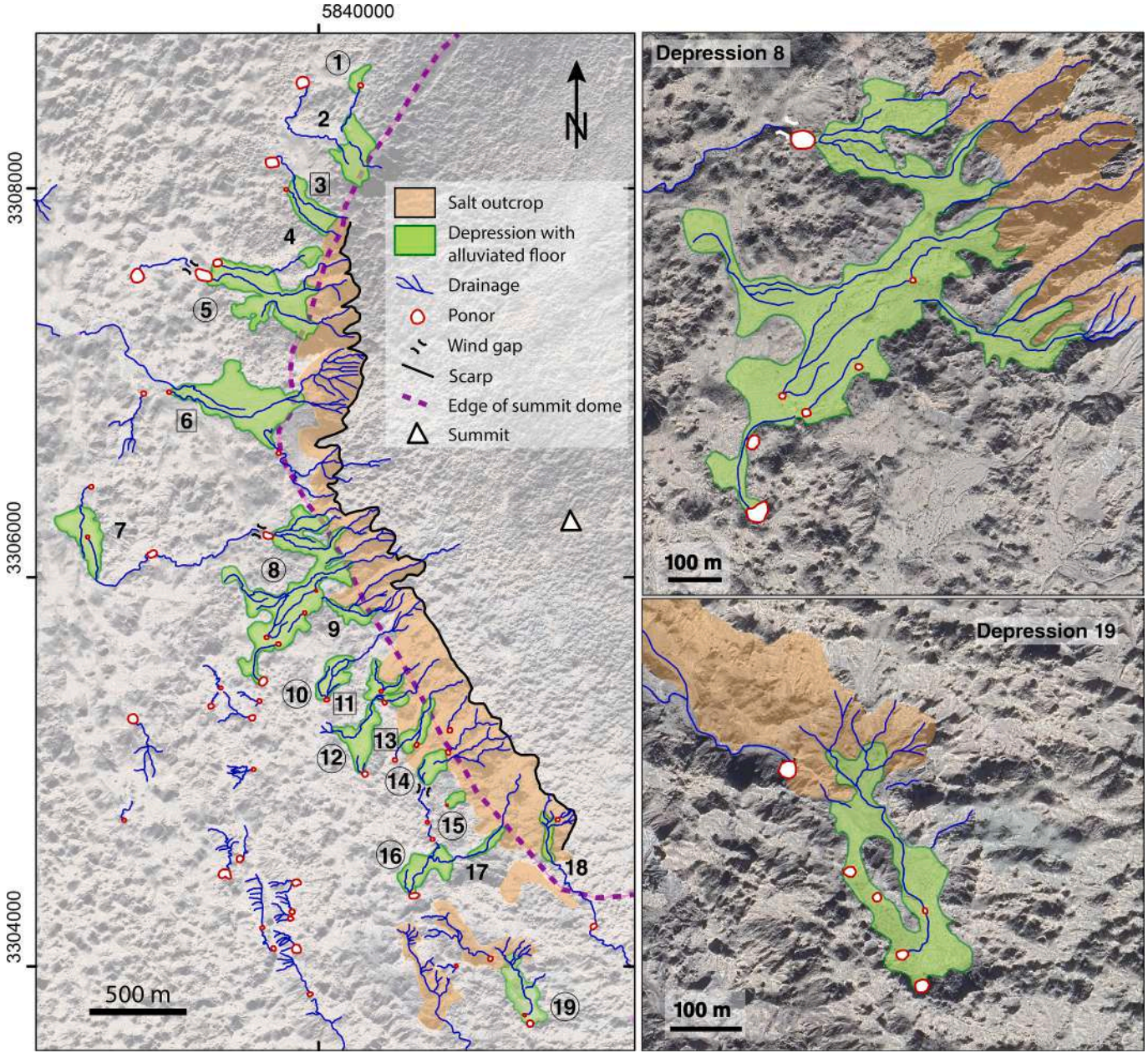

Fig. 4. General geomorphological map of the alluviated depressions mostly associated with the western scarp of the summit dome and detailed map of depressions 8 and 19, corresponding to closed poljes. Closed, semiclosed and open depressions have been differentiated in the general map with circles, squares and no polygon.

Table 1
Typology, drainage and morphometric parameters of the alluviated flat-floored depressions mapped at the foot of the western scarped slope of the summit dome. Numbers corresponds to those indicated in Fig. 4.

Number	Type	Drainage	Area (m^2)	Axial length (m)	Width (m)	Elongation ratio	Orientation
1	Polje	Closed	4605	142	59	2.4	31
2	Piedmont apron	Open	36,096	364	210	1.7	173
3	Polje	Semiclosed	26,574	329	132	2.5	152
4	Piedmont apron	Open	5896	113	81	1.4	82
5	Polje	Closed	88,590	617	324	1.9	122
6	Polje	Semiclosed	106,790	675	310	2.2	93
7	Polje	Semiclosed	36,857	369	181	2.0	168
8	Polje	Closed	142,053	930	465	2.0	13
9	Piedmont apron	Open	9673	249	101	2.5	104
10	Polje	Closed	19,517	266	127	2.1	42
11	Polje	Semiclosed	16,529	270	188	1.4	143
12	Polje	Closed	26,844	355	216	1.6	8
13	Polje	Semiclosed	13,802	293	101	2.9	24
14	Polje	Closed	13,394	186	108	1.7	28
15	Polje	Closed	3116	97	48	2.0	58
16	Polje	Closed	28,604	292	180	1.6	32
17	Valley section	Open	5027	223	40	5.6	51
18	Valley section	Open	6631	253	65	3.9	169
19	Polje	Closed	31,869	371	136	2.7	157

Fig. 5. Panoramic mage of a closed polje (depression 8 in Fig. 4 and Table 1) at the foot of the western steep flank of the summit dome (SD). The flat and gently sloping floor of the basin is underlain by unconsolidated alluvium (A). The main ponor (P) of the depression, a bedrock collapse sinkhole, is located in the lower left of the image. Note landslide scar (LS) on the steep flank of the summit dome at the right.

Table 2
Summary statistics of sinkhole length and area for all the mapped sinkholes in the southern namakier of Jahani salt extrusion, and in selected proximal and distal sectors of the salt glacier (selected sectors shown in Fig. 13).

	Sinkhole length (m)			Sinkhole area (m^2)		
	All	Proximal sector	Distal sector	All	Proximal sector	Distal sector
N. of sinkholes	6489	2106	699	6489	2106	699
Minimum	2.5	3.0	8.2	3.7	5.3	34.3
Maximum	561.3	255.2	443.6	121,275.1	32,399.5	103,922.8
Sum	–	–	–	9,225,635.1	997,616.7	3,461,221.8
Median	21.4	16.7	71.4	230.9	148.2	2743.9
Mean	36.3	23.3	83.1	1421.7	473.7	4951.7
Standard deviation	40.4	21.1	55.1	4131.5	1250.8	7099.1
Skewness	3.0	3.1	1.5	11.6	12.4	5.8
Kurtosis	15.6	17.2	4.5	238.4	247.3	61.3

within the category of closed or semiclosed erosional poljes, in as much as they are carved into karst bedrock mostly by dissolution, display flat alluviated floors and have full or partial internal drainage (De Waele and Gutiérrez, 2022 and references therein). Some of these depressions have very irregular geometries in plan, attributable to the coalescence of adjoining depressions by lateral expansion, and they may also display protruding residual inliers of bedrock in the floor (hums). Some streams that terminate in ponors can be traced further downstream, expressed as wind gaps and beheaded valleys. This evidence reveals the disruption of former longer drainages by the formation of collapse sinkholes.

4.3. Sinkhole analysis

A total of 6489 sinkholes were mapped in a large area covering most of the southern namakier of the Jahani salt extrusion (Fig. 6A). The summit dome of the salt fountain, with a juvenile karst landscape developed on recently emerged salt, has not been included in the mapped area due to the reduced size of the sinkholes, below cartographic resolution. The mapped sector covers 21.62 km^2, which represents 32 % of the salt extrusion (67.89 km^2). It includes two outcrops of non-evaporitic units intercalated within the Hormuz Formation, totalling an area of 1.86 km^2 (8.6 % of the mapped area). The southern and larger

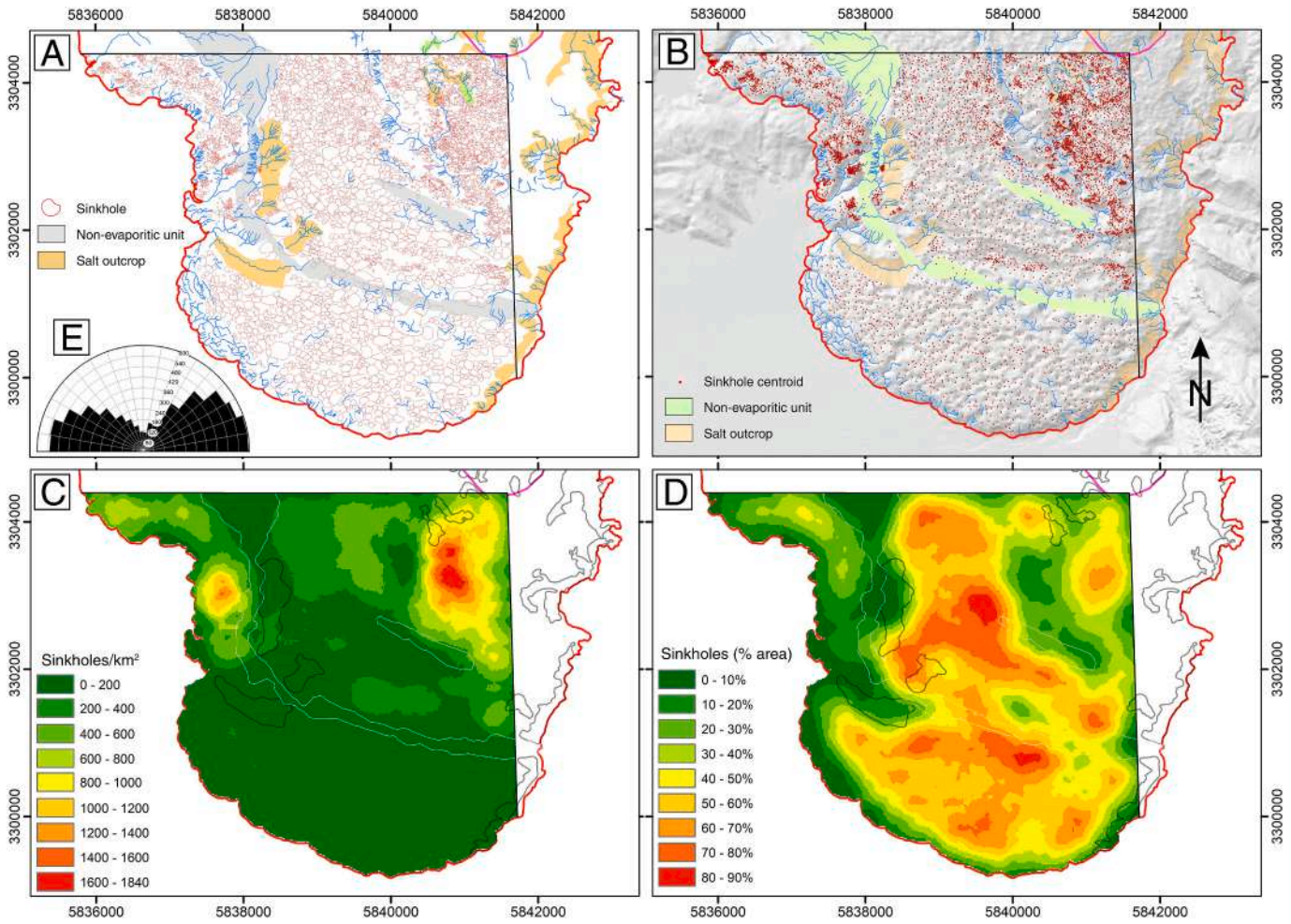

Fig. 6. Distribution of the 6489 sinkholes mapped in the southern namakier of Jahani salt extrusion and density models derived from them. A: Sinkhole map. Grey and orange polygons represent exposures of non-evaporitic rocks and the main salt outcrops, respectively. B: Centroids of the sinkholes on a shaded relief model. Green and orange polygons indicate the distribution of non-evaporitic rocks and the main salt outcrops, respectively. C: Point density model depicting the number of sinkhole centroids per square kilometre, computed with a search radius of 300 m. D: Areal density model showing the percentage area occupied by sinkholes calculated with a search radius of 300 m. Polygons in C and D with white and black outlines indicate exposures of non-evaporitic rocks and salt bedrock. E: Rose diagram with intervals of 10° illustrating the frequency of the orientation of the major axes of the 6489 mapped sinkholes.

band, with an arcuate pattern, reflects the overall recumbent flow-fold structure of the Hormuz Formation in the namakier. The eastern flank of the namakier has been excluded from the analysis because of insufficient quality of the available imagery. The sinkhole edges have been mostly delineated along slope breaks, expressed as changes in shading and vegetation. Frequently, given the polygonal pattern of the depressions in some areas, adjoining sinkholes share boundaries defined as narrow divides. Numerous depressions correspond to compound sinkholes with complex geometries resulting from the coalescence of adjacent depressions. The abundant nested depressions and swallow holes identified in the floor of sinkholes were not mapped to avoid spatial redundancy (Fig. 7D).

The salt extrusion exhibits an extremely high sinkhole density, with an average value of 300 sinkholes/km^2 in the mapped area (Figs. 6A, B, 7A). This mean value rises to 328 sinkholes/km^2 if the outcrops of non-evaporitic rocks are excluded. The inventoried sinkholes have a cumulative area of 9.2 km^2, indicating that at least 41.2 % of the surface is occupied by sinkholes, which are the dominant geomorphic feature in the salt extrusion. Sinkholes display genetic and morphological diversity, as well as a broad range of planimetric dimensions (Fig. 7). The area of the mapped sinkholes reaches a maximum value of 121,275 m^2, and has mean and median values of 1422 m^2 and 238 m^2, respectively. Sinkhole length, given by the length of the straight line between the most distant points of the perimeter (major axis) reaches 561 m, and has average and median values of 99 m and 58 m, respectively. Summary statistics of sinkhole length and area in the mapped area, as well as in selected proximal and distal sectors of the salt glacier (shown in Fig. 13) are presented in Table 2.

Sinkholes mostly occur in relatively flat areas where the salt bedrock is covered by a capsoil. This regolith is typically indurated by cementation and exhibits a brittle rheology (i.e., collapse subsidence). The interface between the capsoil and the salt bedrock is typically well-defined and very irregular, often showing a pinnacled rockhead. Thickness variations in the weathering mantle shows two main spatial trends (Bruthans et al., 2009; Zarei et al., 2012; Abirifard et al., 2017): (1) a general increase towards the distal sector of the salt glacier, where the flowing salt has been subject to dissolutional weathering over progressively longer periods of time; and (2) local variations controlled by the slope, with decreasing thickness towards areas with greater slope, where surface erosion counteracts the production of the dissolution residue in the subsurface. Fig. 8 illustrates the percentage of the slope values for the sinkhole centroids and in all the mapped area. A cell size of (120 m) was considered in the slope computation to obtain an estimate of the general slope of the area surrounding each pixel or point. The graph reveals that sinkholes mostly occur in low gradient areas, where water infiltration is greater and the erosion of the dissolution

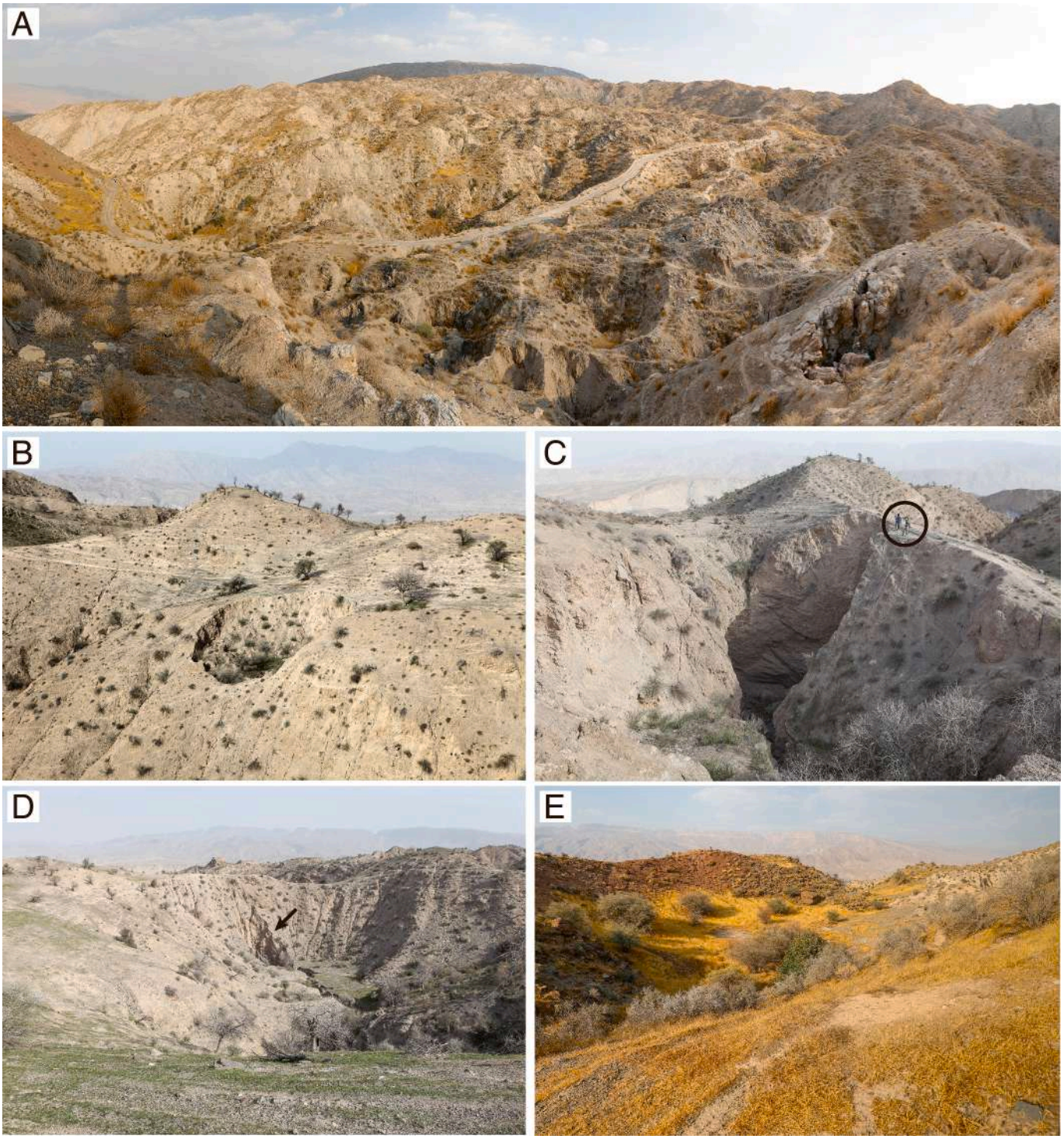

Fig. 7. Images of sinkholes. A: General view of polygonal karst landscape in the NE-directed namakier. Summit dome in the background and collapse sinkholes with unloading cracks in the lower right. B: Fresh-looking collapse sinkholes on a slope underlain by capsoil. C: Cover and bedrock collapse sinkhole with deep shaft in salt bedrock. Circle indicates persons for scale. D: Collapse sinkhole with degraded margins and flat-floored fill with a gully terminating in a nested collapse that functions as a ponor (black arrow). E: Large elongated sinkhole (compound collapse sinkhole) developed at the contact between a reddish non-evaporitic unit (left) and Hormuz salt (right).

residue is less effective, allowing the development of capsoils. The 0–20° slope range includes 75 % of the inventoried sinkholes, whereas that slope interval represents 58.3 % of the mapped area. In case the sinkholes would have a perfectly even distribution independent of slope, the ratio for different slope intervals between the percentage of slope values for sinkhole centroids and the percentage of slope values for the whole mapped area would be around 1. However, this ratio has values of 1.3 for the slope intervals 0–10° and 10–20°, while it shows decreasing values of 0.8, 0.2, 0.05, and 0 for the intervals 20–30°, 30–40°, 40–50°, and 50–60°, respectively.

Collapse is clearly the dominant subsidence mechanism, given the brittle rheology of both the indurated capsoil (cover) and the salt bedrock (i.e., cover collapse sinkholes, cover and bedrock collapse sinkholes). Recent, fresh-looking sinkholes typically display a

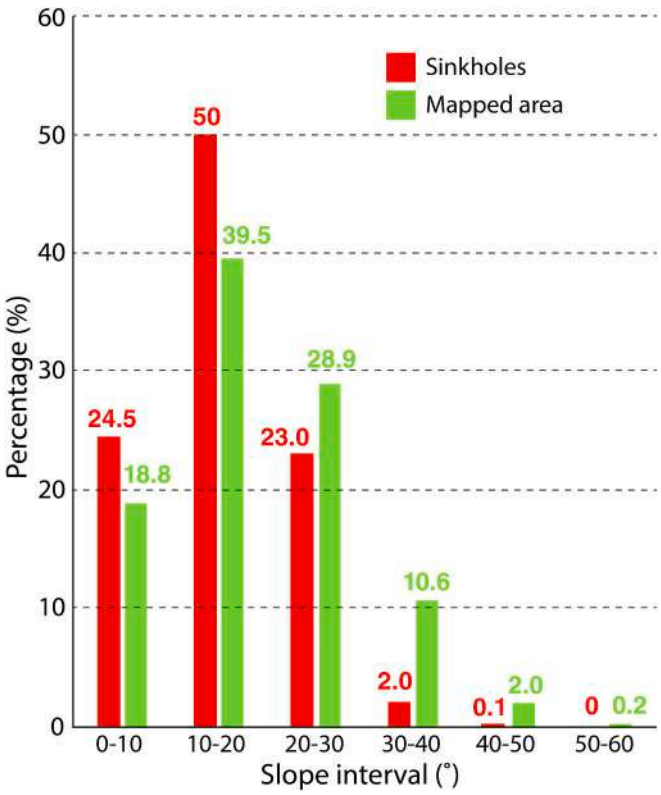

Fig. 8. Percentage of slope values obtained for the 6489 mapped sinkholes and the whole mapped area, showing preferential development of sinkholes in low gradient areas.

cylindrical morphology, with scarped edges and subcircular shape in plan (Fig. 7B, C). Capsoil collapse sinkholes are a few meters across in areas with relatively thin residual capsoil. Single collapse sinkholes may reach tens of meters in diameter. These depressions can be related to collapse of cavities developed within the salt bedrock (capsoil and bedrock collapse sinkholes; Fig. 7C) and to the collapse of voids developed at the rockhead in areas with thick and indurated capsoil (capsoil collapse sinkholes). Collapse sinkholes tend to evolve into much larger depressions by the degradation their slopes affected by erosion, attaining the shape of a cone or a truncated cone (Fig. 7D). This progressive areal expansion can be accompanied by a depth decrease related to the accumulation of a detrital fill in the sinkhole floor, often showing small nested cover collapse and cover suffosion sinkholes (Fig. 7D). The lateral expansion of adjoining sinkholes leads to their coalescence forming compound depressions with more complex geometries, involving an increase in the size of the sinkholes at the expense of the number of sinkholes. This implies a decrease in the sinkhole density by number in parallel with an increase in the area occupied by sinkholes (i.e., areal density) (Fig. 6C, D).

Overall, and in agreement with Zarei and Raeisi (2010) and Abirifard et al. (2017), the mapped sinkholes display a general increase in size towards the distal sector of the namakier, where the surface is riddled by tightly packed depressions mostly with degraded margins, forming a striking example of polygonal karst landscape (Fig. 6A). The graph of Fig. 9 plotting sinkhole length versus radial distance of the sinkhole centroids to the highest point of the summit dome illustrates the general increase in sinkhole size towards the distal sector of the namakier. The upper boundary of the plotted points suggests a maximum sinkhole size for each sector controlled by the distance to the summit dome, and thus the time elapsed since salt emergence. In the southern lobe of the namakier, beyond the arcuate band of non-evaporitic rocks, sinkhole density by number is lower than 200 sinkholes/km^2, whereas the percentage area covered by sinkholes is mostly higher than 50 % and locally reaches 70–90 % (Fig. 6C, D). These figures reflect a mature sinkhole landscape characterised by large depressions with a high degree of coalescence and degraded margins that occupy a great part of the space. The highest sinkhole densities by number occur in the proximal sector of the namakier, just below the summit dome, with values greater 600 sinkholes/km^2, and locally higher than 1600 sinkholes/km^2. Here sinkholes are relatively small, and occupy a great part of the topographic surface, with areal densities mostly above 40 % (Fig. 6C, D). The zone in the proximal sector with low sinkhole density by number and area corresponds to a deeply entrenched blind valley dominated by steep salt outcrops essentially lacking capsoil (Fig. 6C, D). The marginal fringe of the namakier, characterised by external drainage and steep slopes with residual soil dissected by gullies, or salt outcrops (eastern flank), show low sinkhole densities. An apparently anomalous area occurs on the western flank of the namakier, where the salt has surmounted a topographic high in the country rock. This sector, despite of its distal

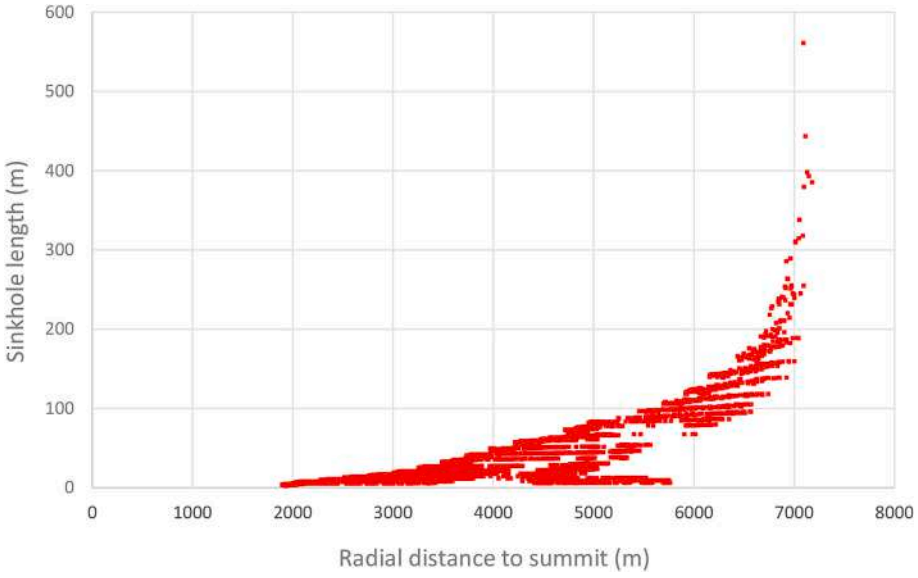

Fig. 9. Graph plotting sinkhole length (major axis) versus distance of the 6489 sinkhole centroids to the crest of the summit dome, showing the increasing size (and age) of the sinkholes towards the distal sector of the salt glacier.

position, displays a high density of small collapse sinkholes mostly developed is relatively flat inter-valley areas with thin capsoil (Fig. 6). The observed pattern can be attributed to the high degree of fluvial incision, which may have contributed to produce some kind of morphological rejuvenation by erosion processes, obliterating pre-existing sinkholes and leading to a new cycle of sinkhole development. Rows of sinkholes are observed along the contacts between the salt and the interbedded non-evaporitic rocks, representing a contact karst favoured by local allogenic drainage derived from the adjacent outcrops of non-karst rocks (Fig. 7E).

The rose diagram of Fig. 6E shows the frequency of the orientation of the major axes of the 6489 sinkholes. The azimuths vary from NW to W and from NE to E, being *E*-W the dominant trend and the N-S orientation lacking. These directions are consistent with the internal structure of the Hormuz salt in the mapped namakier, affected by E-W-oriented folds perpendicular to the flow direction that veer to NW-SE and NE-SW towards the western and eastern flanks of the salt glacier, respectively. The concordance of the sinkhole orientation with the fold trends can be attributed to two factors: (1) dissolution focused on beds more susceptible to dissolution within the Hormuz salt; and (2) deformation of the sinkholes by salt flow, with local shortening directions perpendicular to the flow direction of the salt. The structural control on the sinkholes developed on folded salt is also reflected by the elongation ratio (major axis/minor axis), with average values of 1.45 and 1.41 in the proximal and distal sectors, respectively.

The spatial distribution of the sinkholes and their degree of clustering versus dispersion can be assessed quantitatively computing with the sinkhole centroids the Nearest Neighbor Index (NNI; Clark and Evans, 1954, Williams, 1972; De Waele and Gutiérrez, 2022). This index (NNI = La/Le) corresponds to the ratio between the mean distance between the nearest neighbors within the analysed area (La), and the mean theoretical distance between the nearest sinkholes (Le) in a field with random distribution and the same density (D). The theoretical distance Le is given by $1/(2\sqrt{D})$ (Clark and Evans, 1954). The NNI can range from 0 to 2.1491. A NNI of 0 would indicate maximum aggregation or clustering, not feasible in a real sinkhole field (all centroids share the same location), 1 random distribution, and 2.1491 a uniform pattern that is as evenly and widely spaced as possible. A NNI of 0.77 (z-score − 34.05; *p*-value: 0.0) has been computed for the centroids of the 6489 mapped sinkholes. This value reflects the clustered distribution of the sinkholes in some sectors of the namakier, particularly in the less evolved sinkhole landscape of the proximal zone and especially the western sector. Different values of 1.12 (z-score 6,01; p-value: 0.0) and 0.88 (z-score − 10.48; p-value: 0.0) are obtained when the NNI is computed for the distal sector (699 sinkholes, 6.9 km^2) and the proximal sector (2106 sinkholes, 2.2 km^2), respectively.

4.4. Salt escarpment

The northern salt glacier of Jahani is trimmed by an extraordinary salt escarpment carved by the Firuzabad River, which has been dammed recurrently in the past (Gutiérrez et al., 2025b) (Figs. 10, 11). The crest of the escarpment has a cartographic length of 6 km, and extends along a straight distance of 3.6 km, yielding a sinuosity index of 1.7. The height of the scarp exceeds 200 m along great part of its length, and reaches 426 m in the central sector. The scarp shows two arcuate sections associated with the outer side of meanders of the Firuzabad River. Here, the foot of the slope shows conspicuous evidence of active undercutting by the river flow, which erodes the salt bedrock and slope deposits chiefly made up of salt clasts (i.e., talus, rock falls). Both, the free-face salt scarp and the capsoil-covered slopes above the crest locally display prominent unloading cracks (Fig. 10). The steep rock salt slopes also show fresh rock fall scars, typically coated by a crust of white secondary salt (Fig. 11B). The salt bedrock may be exposed up to the foot of the slope or may be covered by relatively smooth talus slopes or recent rock fall deposits (Fig. 11B, D). The talus slopes mainly consist of gravel-sized clasts of rock salt shed from the free face by small rock falls and reduced in size by dissolution. The rugged rock-falls deposits correspond to disintegrated massive collapses that mainly consist of decimetre- and meter-scale boulders, although they can reach tens of meters in length (Fig. 11B). The boulders experience rapid dissolutional wasting, as indicate their sub-rounded geometry and the presence of abundant

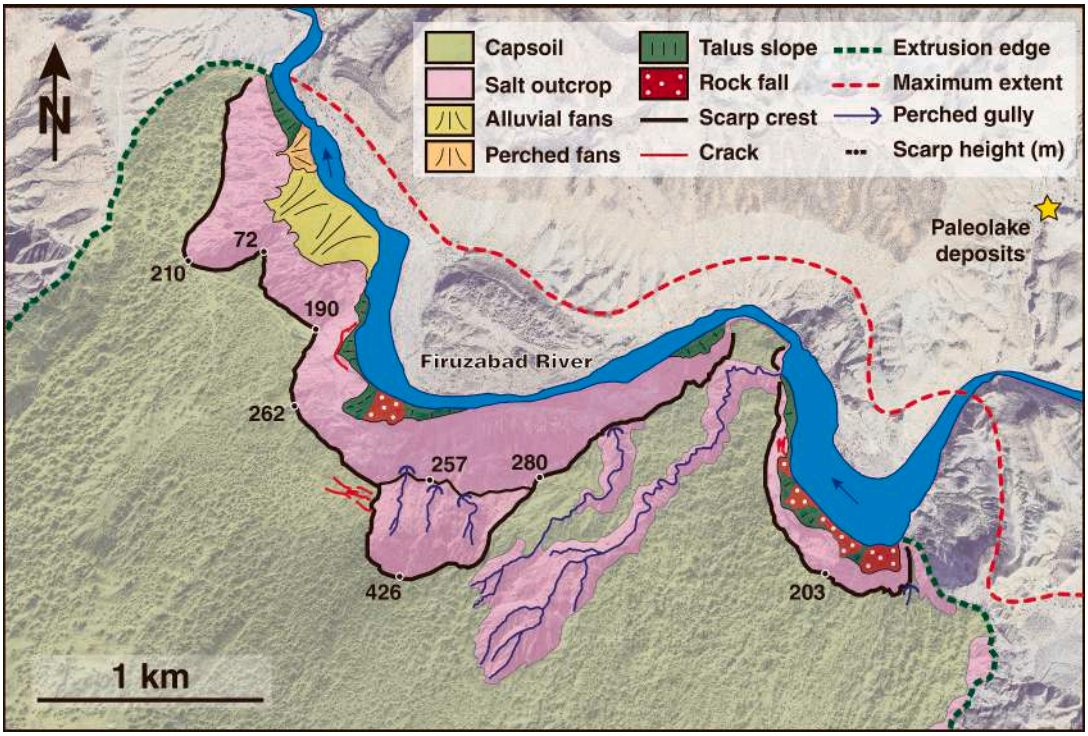

Fig. 10. Geomorphological map of the salt escarpment trimmed by the Firuzabad River in the northern namakier of Jahani.

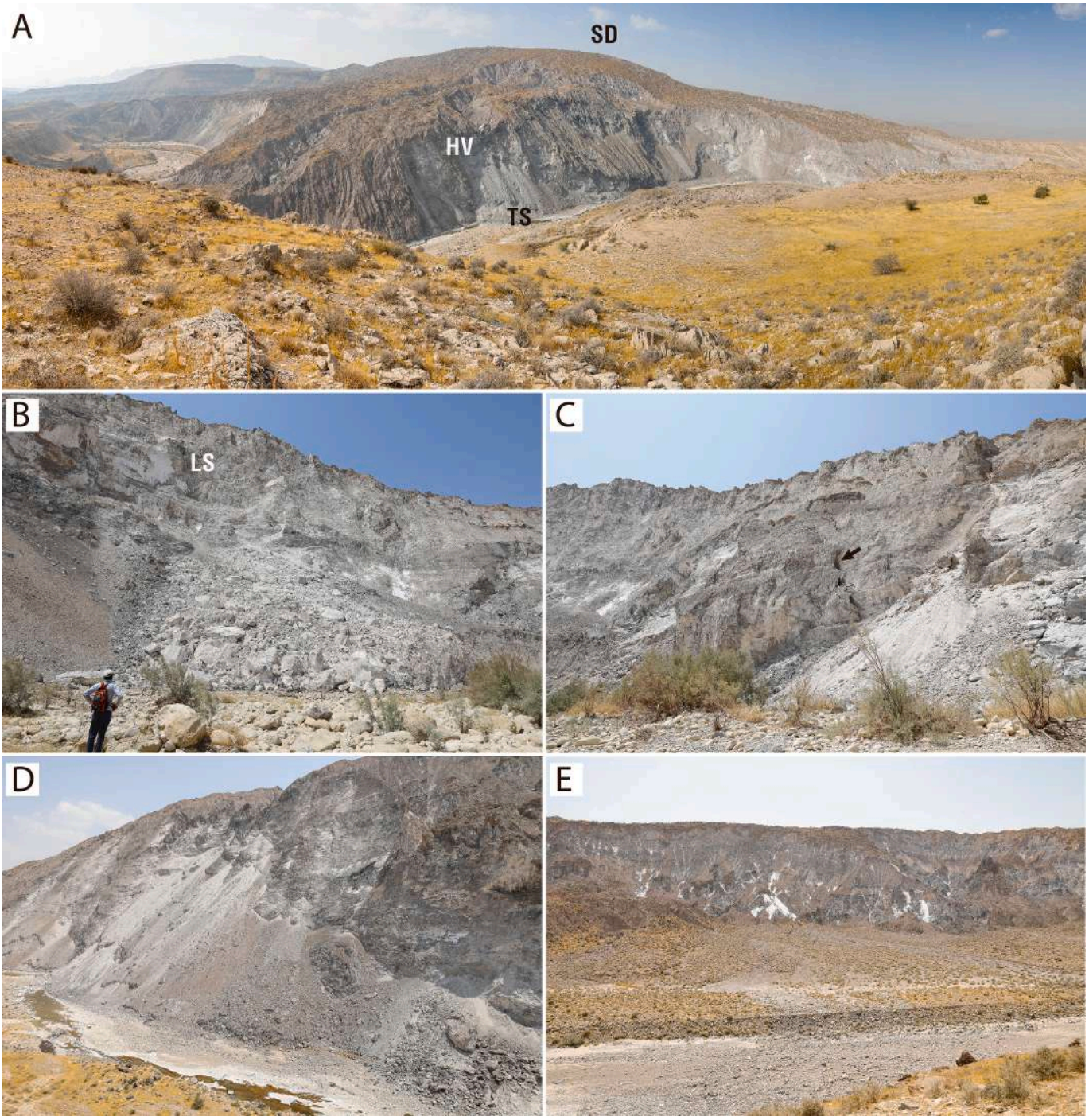

Fig. 11. Images of the salt escarpment trimmed by the Firuzabad River in the northern salt glacier of Jahani. A: General view of the escarpment looking south. SD: Summit dome, HV: Hanging valley, TS: Talus slope mainly consisting of rock salt clasts. B: Rock fall of salt bedrock accumulated in the channel of the Firuzabad River. LS: Landslide scar coated with halite precipitates. C: Scarp over-steepened by fluvial undercutting and affected by unloading cracks (arrow). Bed of the Firuzabad River in the foreground. D: Escarpment with talus slopes mainly consisting of rock salt clasts and affected by fluvial undermining. E: Scarp dissected by a dense gully network that feeds alluvial fans made up of insoluble rocks. The Firuzabad River in the foreground.

karren, notably solution flutes (i.e., rillenkarren). In the western section of the escarpment, associated with a straight stretch of the river, active and perched alluvial fans prevent undercutting at the foot of the scarp (Fig. 11E). Here, the salt escarpment has a lower gradient and is dissected by a dense gully network, indicating a different erosional style dominated by dissolution caused by direct rainfall and runoff. Bedrock dissolution releases clasts of multiple lithologies embedded in the salt (i.e., inclusions) that feed the alluvial fans.

4.5. Salt rimstones

Exceptional halite rimstones were found and examined in February 2012 and September 2023 in a marginal drainage situated along the northern flank of the NW-directed salt glacier lobe (labelled with a green star in Fig. 2) (Fig. 12). The NW-flowing stream runs along 1.2 km between a limestone outcrop to the north (dissected back of a SW-dipping cuesta) and steep slopes on capsoil-covered salt to the south. The drainage has an orographic catchment area of 2.2 km^2, of which 1.2 km^2

Fig. 12. Images of halite rimestones developed in a valley at the margin of the salt extrusion feed by brine springs. A: Rimstone pools with growing sheltstones and coralloids in September 2023 (dry season). B: Image taken in February 2012 (wet season) when water was flowing through holes at the base of the rimstones, affected by dissolutional etching.

correspond to the namakier. The trunk channel within the salt extrusion has two permanent brine springs (Fig. 2). Abirifard et al. (2017) indicate average flow rates of 2.7 and 1.8 l/s for those springs and estimate an average TDS for the brine springs in Jahani of 317 g/l, saturated with respect to halite. A succession of halite rimstone pools occur along an 80 m long section of the valley, accumulated on both limestone bedrock and unconsolidated gravelly alluvium (Fig. 12).

In September 2023 (dry season) the pools were filled with water and halite precipitation was active, while in February 2012 (humid season) the stream water was flowing through holes in the bottom of the rimstones (Fig. 12). A portion of a rimstone collected in 2023 was dissolved for chemical analysis, yielding mass percentages for Na^+ and Cl^- of 59 % and 38.71 % and a Na/Cl molar ratio of 1.01, indicating that around 97.7 % of the deposit correspond to halite. Other minor components included insoluble residue (0.8 %), SO_4^{2-} (0.53 %), HCO_3^- (0.22 %), Ca^{2+} (0.1 %), K^+ (0.1 %) and Mg^{2+} (0.02 %). The rimstone barriers, up to 9 m long and 1.3 m high, display the typical downstream convexity in plan and internal horizontal layering on the upstream side related to episodic vertical aggradation and the development of shelfstones. In September 2023 the rimstone pools displayed (Fig. 12A): (1) inward growing shelfstones; (2) scattered rafts related to evaporative precipitation associated with the water-air interface in the pools; and (3) widespread coralloids ascribable to capillary rise and evaporation. In February 2012 halite deposits exhibited significant dissolutional etching with abundant pitting and a darker dusty surface, which could be related to deposition of airborne particles and concentration of insolubles by dissolution (Fig. 12B).

5. Discussion

5.1. Surface versus subsurface drainage

The Jahani salt extrusion is dominated by a holokarst landscape in which the main morphogenetic process is the development of tightly packed collapse sinkholes. These polygonal karst areas occur in the low-gradient sectors with capsoils, including the upper part of the summit dome and the namakiers (Figs. 6, 7A). The steep slopes on impermeable salt bedrock display a very peculiar fluvial landscape, featuring dense gully networks essentially carved by dissolutional erosion (Fig. 3). Most of the eroded mass in these badland-like areas is transferred downslope in solution, but sufficient insoluble components can be released as solid load to generate alluvial fans (Fig. 11E) and fill large flat-floored depressions (Figs. 4, 5). An exception is found in the salt escarpment undermined by the Firuzabad River, where landsliding largely overwhelms gullying (Fig. 11A). Fluvial dissection also prevails in the frontal zone of the namakiers, where high gradient and relatively thick capsoils inhibit sinkhole development (Fig. 2). Around 19 % of the salt extrusion is dominated by external surface drainage, mainly including the marginal sectors of the namakiers and the salt escarpment. In some sectors of the namakiers the holokarst is substituted by a fluviokarst landscape, with valley networks that terminate in ponors (blind valleys) and valleys disrupted by collapse sinkholes (Figs. 2, 4). Numerous examples of fluvial to karst and karst to fluvial transitions (Phillips et al., 2004; Phillips, 2017) can be observed, such as thalwegs interrupted by sinkholes or sinkholes incorporated into stream networks, respectively. The anomalously long SE-directed stream network developed in the southern glacier and interrupted by numerous collapse sinkholes, might correspond to a cave-collapse valley, as supports its association with a number of caves with similar trend (see cave maps in Bruthans et al., 2024) (Fig. 2).

5.2. Salt karst poljes

A total of 19 large depressions with flat alluviated floors have been mapped in the proximal sector of the western namakier (Fig. 4, Table 1). They are mostly associated with the foot of the steep rock salt slopes of the western flank of the summit dome, dominated by surface runoff and affected by rapid dissolutional erosion (Bruthans et al., 2008, 2017). Four types of depressions have been differentiated on the basis of their morphological and hydrological features: (1) valley sections; (2) piedmont alluvial aprons; (3) semiclosed poljes; and (4) closed poljes (Fig. 5). The valley sections are local widenings in throughgoing valleys, where a deeply entrenched bedrock channel changes locally into a flat-floored valley underlain by alluvium. The development of these valley widenings in a relatively homogeneous bedrock can be related to factors such as a decrease in the slope of the salt extrusion (depression 17 in Fig. 4) that favours lateral channel migration and/or sinkhole coalescence. The piedmont alluvial aprons with throughgoing drainage result from the release of debris from the rapidly eroding salt slopes and its accumulation by sheetfloods in the piedmont area, promoted by the sharp gradient decrease at the junction between the summit dome and the namakier. The semiclosed and closed poljes, which reach around 1 km in length and 14 ha in area, are to our knowledge the first salt karst poljes documented and mapped worldwide (see reviews in De Waele and Gutiérrez, 2022; Gökkaya and Gutiérrez, 2022). Bosák et al. (1999), in a paper mainly focused on caves developed in numerous salt diapirs of the Zagros Mountains, mentioned the presence of “polje-like depressions that represent a special case of blind valleys”, but they neither indicated

their location (e.g., name of salt diapir), nor provided any cartographic information, making impossible to assess the nature of these depressions. The origin of these erosional poljes with full or partial internal drainage can be attributed to the transition of alluvial aprons by differential dissolutional erosion into closed or semiclosed basins. The bedrock underlying the alluvium experiences greater dissolution than the bedrock covered by capsoils in the surrounding areas because of the following factors: (1) potential flooding of the polje floors, especially when runoff exceeds the infiltration capacity by focused and diffuse recharge; and (2) the alluvium has much greater permeability than the capsoils, allowing the rapid transfer of groundwater and preventing significant evapotranspiration. During flood events, typically related to severe storms, water runoff unsaturated with respect to halite infiltrates in the alluvium causing differential dissolutional lowering of the rockhead. Additionally, groundwater in the alluvial aquifer and floodwaters can cause both mechanical and solutional erosion at the margins of the depression leading to the expansion of the basin, as suggests the oversteepened margins of the depressions (i.e., lateral planation by rim dissolution). Flooding is expected to have greater morphogenetic impact in closed poljes than in semiclosed poljes, where it can reach higher magnitude and longer duration. Bruthans et al. (2017), during a flash flood in Jahani, measured a TDS of 47 g/l in runoff derived from salt slopes, indicating that the surface water was far from saturation. Internal drainage in these poljes may occur by diffuse infiltration through the alluvium or via focused recharge at collapse sinkholes (i.e., ponors). Other processes that may also play some role in the development of these poljes include: (1) the continuous lateral spreading of the salt glaciers, which may contribute to the enlargement of the basins in the flow direction; and (2) local subsidence in the proximal sector of the namakiers related to extensional salt flow, as shown by DInSAR data (Gutiérrez et al., 2025b), which might be related to irregularities and slope changes in the "subglacial" topography. The salt karst poljes documented at Jahani salt extrusion has some resemblance with the piedmont poljes described in carbonate karst areas, occurring at the foot of mountainous terrain that supply large amounts of runoff and detrital deposits (Gams, 1994). They also have some similarity with border poljes developed by differential erosion in carbonate rocks in contact with non-karst impervious rocks (De Waele and Gutiérrez, 2022). The difference in this case is that runoff does not come from impervious non-karst terrain (allogenic runoff), but mainly from impervious salt bedrock.

5.3. Sinkholes and polygonal karst

The Jahani salt fountain displays a special sinkhole-dominated karst landscape (polygonal karst) developed on highly soluble rock salt (equilibrium solubility 356 g/l) moving at rates of the order of cm/yr (Gutiérrez et al., 2025b) and affected by flow folding (Talbot et al., 2000) (Figs. 6, 7). This polygonal karst landscape consists of tightly-packed collapse sinkholes, while polygonal karsts in carbonate and gypsum terrains are typically related to solution sinkholes (Williams, 1972; Gökkaya et al., 2021; De Waele and Gutiérrez, 2022). An average sinkhole density of 300 sinkholes/km^2 has been calculated in the mapped area of the southern namakier (6489 sinkholes in 21.62 km^2), significantly higher than the density of 73 sinkholes/km^2 estimated by Abirifard et al. (2017) based on an incomplete sinkhole inventory. The sinkhole density at Jahani is one of the highest documented in the literature (see review in De Waele and Gutiérrez, 2022). Sinkholes mostly develop in low-gradient areas where the salt bedrock is covered by capsoil with high infiltration capacity (Bruthans et al., 2017); 75 % of the mapped sinkholes occur in areas with slopes within the 0–20° range (Fig. 8). Here, subsurface drainage dominates, while in steep slopes on bare and impervious rock salt water infiltration is negligible. Collapse sinkholes are the dominant genetic type (i.e., brittle rheology), and subsidence may affect the indurated capsoil or both the bedrock and the capsoil, depending on whether dissolution acts at the pinnacled rockhead or within the salt bedrock.

In agreement with studies conducted in Jahani (Abirifard et al., 2017) and Konarsiah salt extrusions (Zarei and Raeisi, 2010), sinkholes in the proximal and distal sectors of the namakiers show contrasting differences (Fig. 13A). The observed gradation reflects the time elapsed since the salt was exposed to dissolution, with a juvenile landscape in the recently emerged salt in the summit dome and proximal sectors of the namakier and a mature landscape in the distal sectors. The evolution trend mainly involves the enlargement of the depressions by degradation of their margins, eventually leading to sinkhole coalescence, resulting in a landscape with progressively larger sinkholes with lower sinkhole density by number and thicker capsoil (De Waele and Gutiérrez, 2022; Sevil and Gutiérrez, 2023). Average lengths of 23 m and 83 m have been computed for the sinkholes in the proximal and distal sectors, while densities change from 600 to 200 sinkholes/km^2, respectively. Moreover, the NNI indicates a more uniform distribution of sinkholes in the distal and older portion of the namakier, which is a typical feature of mature polygonal karst landscapes (Williams, 1972). Interestingly, distance from the salt spelling zone (summit dome) represents a proxy for the age of the karst topography in the salt glacier, which displays a continuous morphological evolutionary sequence (Fig. 9).

The comprehensive sinkhole inventory with morphometric data constructed in this work allows comparing the size distribution of the sinkholes in the different sectors of the salt glacier and with that of the sinkholes developed other karst settings. The graph in Fig. 13B plots sinkhole length (major axis) in logarithmic scale versus cumulative frequency of sinkholes equal or larger than a given length in the southern namakier of Jahani, in selected proximal and distal sectors of the salt glacier, as well as in a various types of karst environments (limestone, gypsum and salt; covered, bare and interstratal; epigene and hypogene): (1) cover collapse sinkholes in the limestone karst of Val d'Orleans mantled by weak and thin alluvium (Gombert et al., 2015); (2) single and compound cover collapse and sagging sinkholes in the mantled eogenetic salt karst of the Dead Sea, where depressions experience significant expansion by mass wasting acting on their margins (Sevil and Gutiérrez, 2023); (3) multiple types of subsidence sinkholes developed on alluvium and various caprocks (marls, sandstones, basalts) in the epigene evaporite karst of the Fluvia Valley, NE Spain (Gutiérrez et al., 2016); (4) cover subsidence sinkholes in the limestone karst with a thick cohesive cover in the Hamedan Plains, Zagros Mountains, mostly induced by groundwater withdrawal (Taheri et al., 2015); (5) mainly caprock collapse sinkholes in the deep-seated hypogene interstratal karst of the Sant Miquel valley, NE Spain (Gutiérrez et al., 2019); (6, 7) cover subsidence sinkholes and bedrock collapse sinkholes in the Sivas gypsum karst, Turkey, the latter of which reach exceptionally large dimensions due coalescence and post-collapse expansion by erosion (Gökkaya et al., 2021); and (8) single caprock collapse sinkholes associated with the monoclinal scarp developed atop the dissolution front of the Arab and Hith anhydrite in Saudi Arabia (Gutiérrez et al., 2025a). The length of all the sinkholes mapped in Jahani shows a broad range covering 2.3 orders of magnitude (Table 2), and follows a power-law distribution for great part of the size spectrum. The upper and lower roll-overs are likely related to the incompleteness of the inventory for small sinkholes and the presence of large compound depressions with degraded margins, respectively. The broad size range and the existence of sinkholes as much as 561 m long, despite the relatively low mechanical resistance of the bedrock and the overlying residual deposits, can be attributed to the presence of sinkholes at different evolutionary stages, from small recently formed collapse sinkholes, to large compound depressions resulting from the expansion and coalescence of sinkholes. Compared with sinkholes in other evaporite karsts, the sinkholes in Jahani are larger than those mapped in the salt karsts of the Dead Sea (Sevil and Gutiérrez, 2023) and Ambal dome (Gutiérrez and Lizaga, 2016). These differences can be largely ascribed to the variable strength and thickness of the materials situated above the cavities. The sinkholes in the proximal and distal sectors of the salt glacier show

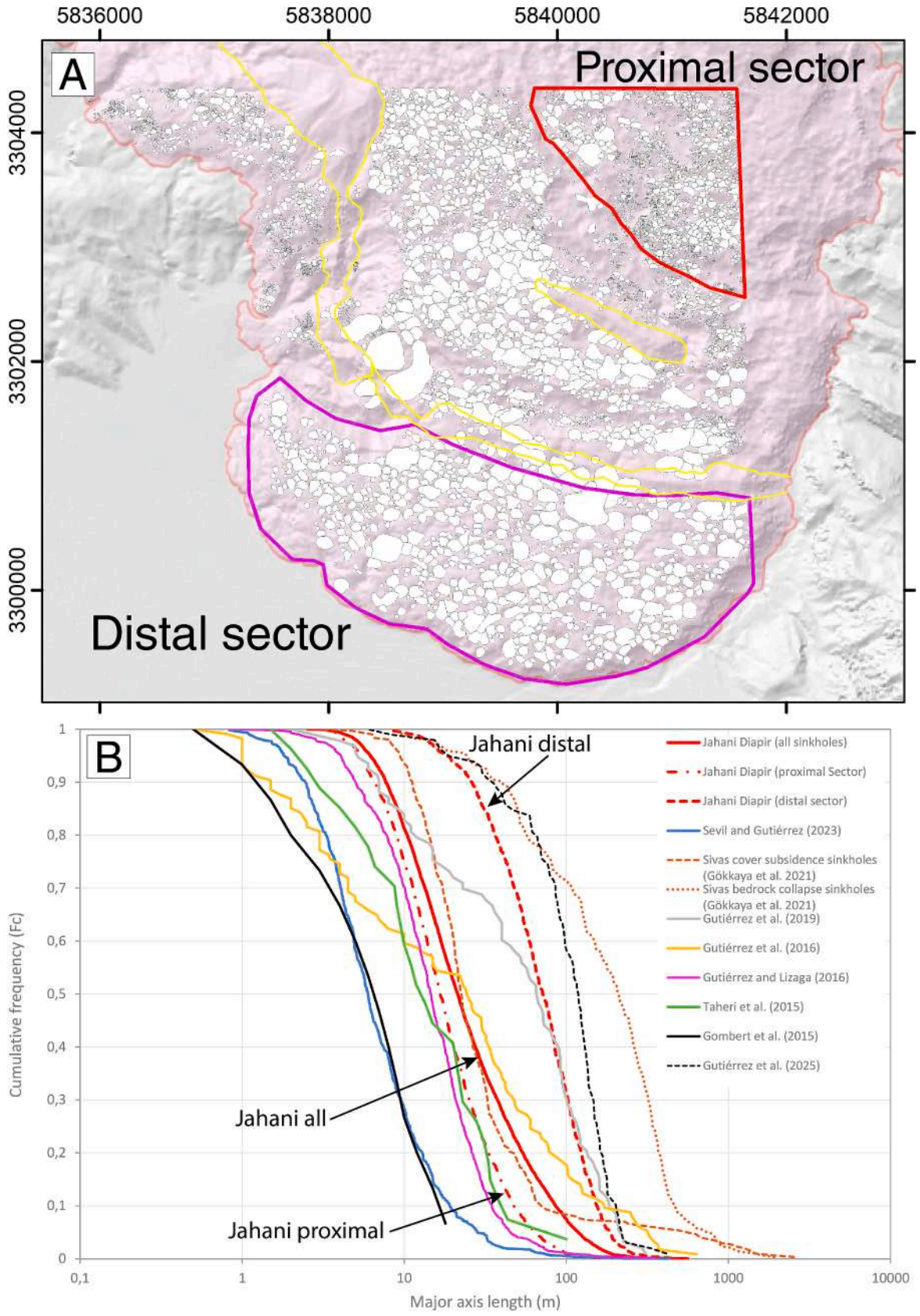

Fig. 13. A: Sinkhole map showing the selected proximal and distal sectors in Jahani. Polygons with yellow outlines indicate exposures of non-evaporitic rocks. B: Graphs of sinkhole length versus cumulative frequency (frequency of sinkholes equal or larger than a given dimension) in the southern salt glacier of Janahi salt extrusion (all, proximal sector, and distal sector) and in a various types of karst environments (carbonate, gypsum and salt; covered, bare and interstratal; epigene and hypogene). See explanation in text.

markedly different cumulative frequency-size distributions, with much larger lengths in the latter. The proximal sinkholes show a distribution similar to those in Ambal dome, lacking spreading salt glaciers (Gutiérrez and Lizaga, 2016), whereas the more evolved distal sinkholes are larger than the caprock collapse sinkholes of the hypogene evaporite karst of Sant Miquel (Gutiérrez et al., 2019), but smaller than the giant bedrock collapse sinkholes of the Sivas gypsum karst (Gökkaya et al., 2021), and the caprock collapse sinkholes of central Saudi Arabia (Gutiérrez et al., 2025a).

A number of features, including the extremely high density of sinkholes some deeply rooted in bedrock, the presence shafts and caves at depths ≥75 m (Abirifard et al., 2017; Bruthans et al., 2024) (Fig. 7C), and permanent brine springs situated at the foot of high-relief salt scarps (Abirifard et al., 2017) (Fig. 3), indicate that the mobile salt mass has a significant conduit permeability within a thick karstification zone. This factual evidence constrasts with the concept proposed by some authors, whereby dissolution in diapirs is restrictred to just a few meters below the surface, arguing that voids and fissures are rapidly annealed by creep deformation (Talbot and Pohjola, 2009). This observation has important practical implications, in as much as salt diapirs a currently one of the main targets for various types of geostorage (e.g., Tackie-Otoo and Haq, 2024). This feature is nicely illustrated by artificial exposures in the nearby Konarsiah diapir, including a highly pinnacled rockhead with conduits and deep-penetrating sediment filled grikes (Fig. 14).

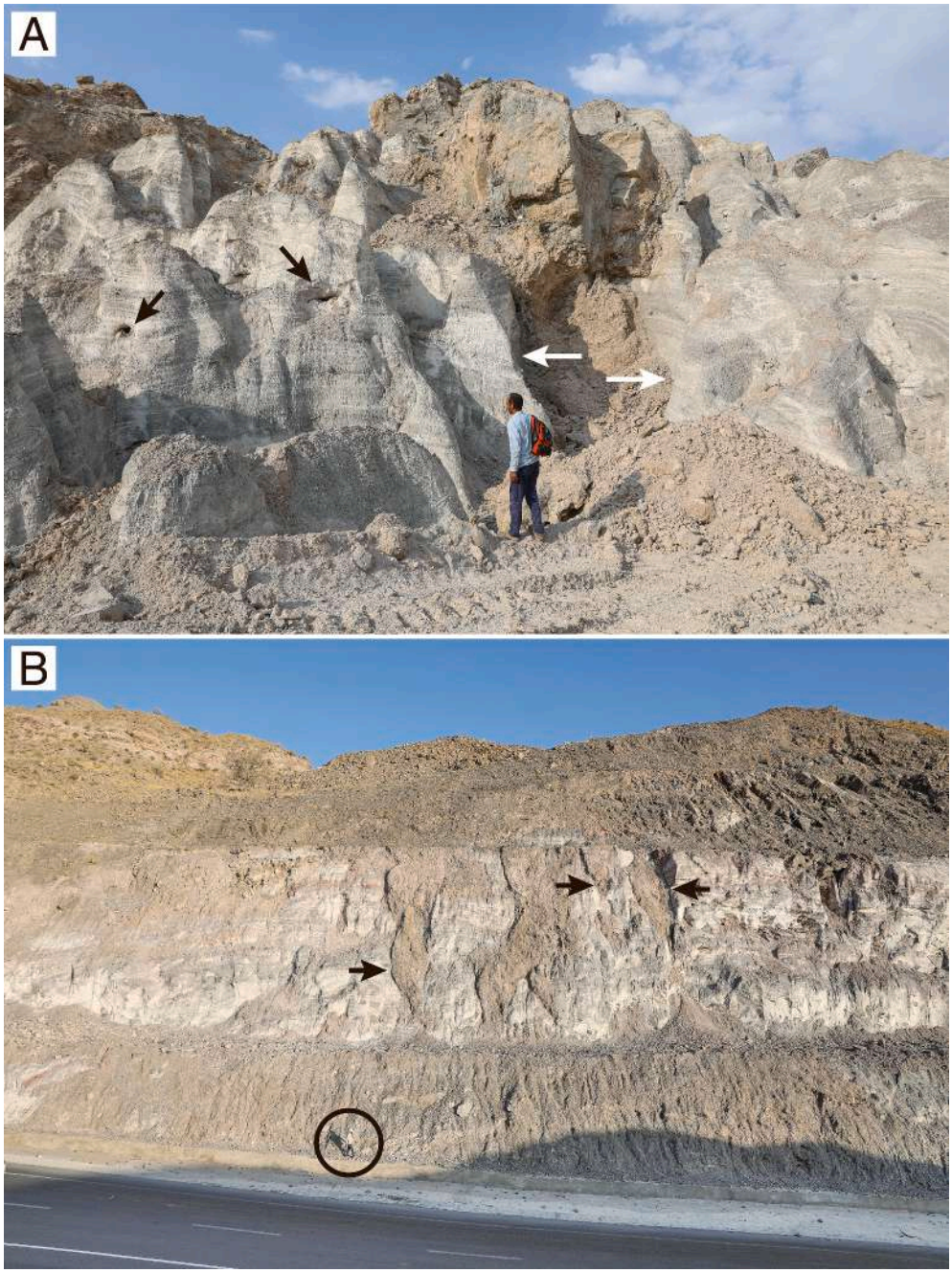

Fig. 14. Subsurface dissolutional features in Konarsiah diapir exposed by artificial excavation. A: Pinnacled rockhead with air-filled (black arrows) and sediment-filled (white arrows) conduits exhumed in a salt mine. B: Cutting in the Firuzabad-Farashband showing decametre-scale, downward-tapering dissolutional conduits (i.e., grikes) in salt bedrock, overlain by caprock. Circle indicates a person for scale.

5.4. The salt escarpment

The 6 km long and up to 426 m high salt escarpment at the front of the northern namakier and associated with the Firuzabad River, is likely the largest salt escarpment on Earth (see review on evaporite escarpments in De Waele and Gutiérrez, 2022). Sometime after 15 ka, the northern salt glacier dammed the Firuzabad valley. Eventually, the river breached the namakier dam. This process probably occurred through the development of a natural tunnel by "subglacial" flows promoted by the highly permeable alluvium, and its progressive collapse to form a cave-collapse valley (Gutiérrez et al., 2025b). At the present time, the escarpment shows evidence of fast retreat (e.g., hanging valleys; Figs. 10, 11A), capable of counterbalancing the rapid flow of the salt glacier towards the valley. According to DInSAR data, the northern salt glacier cascades towards the Firuzabad Valley at horizontal and vertical rates of around −10 cm/yr and 15 cm/yr, respectively (Gutiérrez et al., 2025b). The following processes contribute to the rapid retreat of salt escarpment (Gutiérrez et al., 2023): (1) potential over-steepening of the slope by more rapid flow in the upper part of the salt glacier than in its basal zone, causing outward rotation; (2) development of stress release cracks in the laterally unconfined rock salt mass (Fig. 11C); (3) dissolutional widening of the unloading cracks by infiltration water and salt-crystallisation pressure induced by evaporation (Fig. 11B); (4) rock falls of a wide range of dimensions (Fig. 11B, D); (5) rapid removal of the rock fall debris by stream water; (6) undermining of the slope by fluvial erosion; and (7) dissolutional erosion of the salt bedrock exposures by rainfall and runoff. A critical feature associated with the dynamics of escarpments on evaporite rocks associated with rivers, is that the debris accumulated at the foot of the slope can be readily removed by dissolution, reducing its protecting effect against fluvial undermining (Gutiérrez et al., 2023).

The rapid mass transfer from the advancing escarpment to the river as dissolved salt is dramatically illustrated at Jahani. Abirifard et al. (2017) obtained discharge and hydrochemical data over eight months from two stations in the Firuzabad River situated upstream and downstream of the northern namakier of Jahani (labelled at R1 and R2 in Fig. 1; average TDS of 762 mg/l and 13,451 mg/l, respectively). Between stations R1 and R2 the average concentration of dissolved halite increased from 100 mg/l to 12,070 mg/l, and the total annual mass of dissolved halite from 2520 to 319,725 t (re-calculated for 12 months). Around 75 % of the yearly increase in dissolved NaCl (237,903 out of 317,205 t) is ascribed to dissolution caused by the Firuzabad River along the escarpment, and most of the rest to brines derived from three permanent springs in the NW sector of the extrusion (Fig. 2). Abirifard et al. (2017) indicate that diversion of the river would significantly mitigate the hydrochemical degradation of the river water, but it would cause a significant aesthetic impact adversely affecting the nomination of the diapir for UNESCO World Heritage Site.

5.5. Halite rimstones

A marginal stream displays a succession of large halite rimstone pools (Fig. 12). Calcite rimstones are relatively common in caves and subaerial conditions (Palmer, 2007). However, halite rimstones are mostly small and/or spatially restricted. To our knowledge no examples of comparable size and aesthetic value have been documented in the literature so far. Similar rimstones but with much smaller extent have been reported in Namakdan diapir, associated with a brine spring at the outlet of 3 N cave (Amrikazemi and Sayedyounesi, 2025). The development of these extraordinary rimstones can be attributed to the fact that the flow of the stream with a small catchment (2.2 km^2) is largely supplied by two permanent springs of brines saturated with respect to halite. During dry periods, the saturated brine flowing along the creek contributes to the built up of the rimstones, fostered by evaporation. Runoff related to rain events can dilute the stream flow leading to the partial destruction of the rimstones. However, given the limited size of the watershed and the high infiltration capacity of the ground (capsoils and limestone), severe flash floods capable of destroying the rimstones should be very infrequent. Consequently, the rimstones pools may experience repeated cycles of water ponding and construction, partial destruction and drainage, and self-reparation.

6. Conclusions

The geomorphology and hydrology of the Jahani salt extrusion is largely controlled by the general slope gradient, primarily governed by the overall morphology of the salt fountain, and secondarily by marginal scarps related to fluvial undermining. The low-gradient areas with capsoil in the summit dome and the salt glaciers are dominated a polygonal karst landscape of densely packed collapse sinkholes (holokarst). On the steep slopes, mostly lacking capsoil, the landscape is dominated by badland-like gully networks carved in rock salt. An exception is a great part of the salt escarpment trimmed and undermined by the Firuzabad River, where slope movements overwhelm fluvial dissection. In some sectors of the salt glaciers the polygonal karst is replaced by a fluvio-karst landscape and poljes, which occur at the foot of the bare steep flanks of the summit dome. Runoff prevails in the steep and bare salt slopes, while it is very limited in the areas underlain by capsoil and riddled by sinkholes. The external drainage (ca. 19 %) is restricted to steep frontal zones of the namakiers and the marginal salt scarps.

Poljes with flat floors underlain by alluvium up to 1 km long have developed at the foot the steep rock salt slopes in the flank of the summit dome. To our knowledge, these are the first documented and mapped salt karst poljes. The debris released from the salt slopes by rapid dissolutional erosion accumulate in the proximal sector of the namakier, generating alluvial aprons with troughgoing drainage. These piedmont aprons can evolve into poljes by enhanced bedrock dissolution beneath high-permeability alluvium with a large contributing area, and may also expand by surface and subsurface rim dissolution.

Jahani, like other salt fountains of the Zagros Mountains, displays a very special sinkhole landscape developed on high-solubility salt bedrock that is continuously emerging at the surface and experiencing displacement at rates of the order of cm/yr, as well as internal deformation (i.e., flow folding). Sinkholes in this mobile karst terrain exhibit a morpho-chronological gradation, changing from a youthful landscape of small sinkholes developed on recently spelled salt, to a mature landscape with much larger sinkholes related to expansion and coalescence processes. A comprehensive inventory of 6489 sinkholes with morphometric data has allowed to quantitatively characterise sinkholes in the proximal and distal sectors of a namakier, and compare them with those developed in other karst settings. Sinkholes in the proximal sector reach an exceptionally high density of around 600 sinkholes/km^2. In the distal sector sinkholes have an average length four times larger than in the proximal sector and reach lengths (>500 m) comparable with those reported for giant sinkholes with degraded margins in bare and interstratal Ca-sulphate karst environments.

The Firuzabad River has trimmed the northern namakier of Jahani generating an extraordinary salt escarpment 6 km long and > 400 m high, which is likely the largest salt escarpment on Earth. The escarpment, despite that rapid forward and downward flow of the salt (ca. 15 cm/yr and − 10 cm/yr), shows evidence of long-term retreat (e.g., former river damming, hanging valleys). The current dynamics of the salt scarp in mainly controlled by processes such as over-steepening related to salt flow and fluvial undermining, stress release, high-frequency rock falls, and rapid removal of the rock salt debris by river waters. The scarp is the main source of the dissolved salt responsible for the severe hydrochemical degradation of the Firuzabad River.

Halite rimstones with exceptionally large size and extent occur in a marginal stream. The development of these rimstone pools with remarkable aesthetic value is favoured by the fact that the stream, with a small catchment, is mainly fed by two permanent brine springs of water

saturated with respect to halite. The rimstone pools experience phases of growth, dissolutional degradation and drainage, and self-reparation controlled by the rainfall regime.

CRediT authorship contribution statement

Francisco Gutiérrez: Project administration, Methodology, Investigation, Funding acquisition, Formal analysis, Data curation, Conceptualization, Writing – original draft. **Issa Ilyati:** Investigation, Writing – review & editing. **Mehdi Zarei:** Data curation, Conceptualization, Writing – review & editing.

Declaration of competing interest

The authors declare the following financial interests/personal relationships which may be considered as potential competing interests: Francisco Gutierrez reports financial support was provided by University of Zaragoza. Francisco Gutierrez reports a relationship with University of Zaragoza that includes:. If there are other authors, they declare that they have no known competing financial interests or personal relationships that could have appeared to influence the work reported in this paper.

Acknowledgements

The authors are very grateful to Prof. Mohsen Rezaei for logistical assistance and Dr. Luis Auqué and Dr. María José Gimeno for their advice on halite precipitation and the formation of rimstones. We are very grateful to two anonymous reviewers for their insightful comments. The work has been supported by the Salvador de Madariaga grant (PRX22/00029) and project DIAPERNO (PID 2021-123189NB-I00) of the Spanish Government (Ministerio de Ciencia e Innovación). The TanDEM-X digital elevation models were provided by the German Aerospace Center (grant DEMGEOL288).

Data availability

Data will be made available on request.

References

Abirifard, M., Raeisi, E., Zarei, M., Zare, M., Filippi, M., Bruthans, J., Talbot, C.J., 2017. Jahani Salt Diapir, Iran: hydrogeology, karst features and effect on surrounding environment. Int. J. Speleol. 46, 445–457.

Aftabi, P., Roustaie, M., Alsop, G.I., Talbot, C.J., 2010. InSAR mapping and modelling of an active Iranian salt extrusion. J. Geol. Soc. Lond. 167 (1), 155–170. https://doi.org/10.1144/0016-76492008-165.

Amrikazemi, A., Sayedyounesi, S. 2025. Geoconservation in Iran: Namakdan salt caves. In: Reynard, E. (Ed.)., Geoheritage. Elsevier, Amsterdam, (in press).

Authemayou, C., Chardon, D., Bellier, O., Malekzadeh, Z., Shabanien, E., Abbassi, M., 2006. Late Cenozoic partitioning of the oblique plate convergence in the Zagros fold-and-thrust belt (Iran). Tectonics 25, TC3002.

Authemayou, C., Bellier, O., Chardon, D., Benedetti, L., Malekzade, Z., Claude, C., Angeletti, B., Shabanian, E., Abbassi, M.R., 2009. Quaternary slip-rates of the Kazerun and the Main recent Faults: active strike-slip partitioning in the Zagros fold-and-thrust belt. Geophys. J. Int. 178, 524–540.

Bachmanov, D.M., Trifonov, V.G., Hessami, K.T., Kozhurin, A.I., Ivanova, T.P., Rogozhin, E.A., Hademi, M.C., Jamali, F.H., 2004. Active faults in the Zagros and Central Iran. Tectonophysics 380, 221–241.

Berberian, M., 1995. Master "blind" thrust faults hidden under the Zagros folds: active basement tectonics and surface morphotectonics. Tectonophysics 241, 193–224.

Bosák, P., Bruthans, J., Filippi, M., Svoboda, T., Šmíd, J., 1999. Karst and caves in salt diapirs, SE Zagros Mts. (Iran). Acta Carsol. 28, 41–75.

Bruthans, J., Asadi, N., Filippi, M., Vilhelm, Z., Zare, M., 2008. A study of erosion rates on salt diapir surfaces in the Zagros Mountains, SE Iran. Environ. Geol. 53, 1079–1089.

Bruthans, J., Filippi, M., Asadi, N., Zare, M., Slechta, S., Churackova, Z., 2009. Surficial deposits on salt diapirs (Zagros Mountains and Persian Gulf Platform, Iran): Characterization, evolution, erosion and the influence on landscape morphology. Geomorphology 107, 195–209.

Bruthans J. Filippi M. Zare M. Churáčková Z. Asadi N. Fuchs M. Adamovič J. 2010 Evolution of salt diapir and karst morphology during the last glacial cycle: effects of sea-level oscillation, diapir and regional uplift, and erosion (Persian Gulf, Iran) Geomorphology 121 3–4 291 304.

Bruthans, J., Kamas, J., Filippi, M., Zare, M., Mayo, A.L., 2017. Hydrogeology of salt karst under different cap soils and climates (Persian Gulf and Zagros Mts., Iran). Int. J. Speleol. 46, 303–320.

Bruthans, J., Filippi, M., Slavík, M., Závada, P., Zare, M., 2024. Rapid evolution of salt glacier caves on a mountain diapir in a semiarid climate. Geomorphology 448, 109058.

Clark, P.J., Evans, F.C., 1954. Distance to nearest neighbor as a measure of spatial relationships in populations. Ecology 35, 445–453.

Cvijić, J., 1893. Das Karstphänomen. Versuch einer morphologischen Monographie, Geographische Abhandlungen herausgegeben von A. Penck, Wien, Band V, Heft 3, 1–114.

De Waele, J., Gutiérrez, F. 2022. Karst hydrogeology, geomorphology and caves. Wiley, 888 pp.

Dooley, T.P., Schreurs, G., 2012. Analogue modelling of intraplate strike-slip tectonics: a review and new experimental results. Tectonophysics 574-575, 1–71.

Faghih, A., Nezamzadeh, I., Kusky, T., 2016. Geomorphometric evidence of an active pop-up structure along the sabzpushan fault zone, Zagros mountains, SW Iran. J. Earth Sci. 27, 945–954.

Gams, I., 1994. Types of the poljes in Slovenia, their inundations and land use. Acta Carsol. 23, 285–302.

Ghassemi, M.R., Roustaei, M., 2021. Salt extrusion kinematics: insights from existing data, morphology and InSAR modelling of the active emergent Anguru diapir in the Zagros fold and thrust belt, Iran. J. Geol. Soc. 178 (6), jgs2020-136. https://doi.org/10.1144/jgs2020-136.

Gökkaya, E., Gutiérrez, F., 2022. Poljes in the Sivas gypsum karst. Turkey. Geomorphology 417, 108451.

Gökkaya, E., Gutiérrez, F., Ferk, M., Görüm, T., 2021. Sinkhole development in the Sivas gypsum karst. Turkey. Geomorphology 386, 107746.

Gombert, P., Orsat, J., Mathon, D., Alboresha, R., Al Heib, M., Deck, O., 2015. Role des effondrements karstiques sur les desordres survenus sur les digues de Loire dans le Val D'Orleans (France). Bull. Eng. Geol. Environ. 74 (1), 125–140.

GSI, 1996. Geological Map of Iran 1:100.000 series. Darenjan Sheet. Geological Survey of Iran. Tehran.

Gutiérrez, F., Lizaga, I., 2016. Sinkholes, collapse structures and large landslides in an active salt dome submerged by a reservoir: the unique case of the Ambal ridge in the Karun River, Zagros MountainsIran. Geomorphology 254, 88–103.

Gutiérrez, F., Fabregat, I., Roqué, C., Carbonel, D., Guerrero, J., García-Hermoso, F., Zarroca, M., Linares, R., 2016. Sinkholes and caves related to evaporite dissolution in a stratigraphically and structurally complex setting, Fluvia Valley, eastern Spanish Pyrenees. Geological, geomorphological and environmental implications. Geomorphology 267, 76–97.

Gutiérrez, F., Fabregat, I., Roqué, C., Carbonel, D., Zarroca, M., Linares, R., Yechieli, Y., García-Arnay, A., Sevil, J., 2019. Sinkholes in hypogene versus epigene karst systems, illustrated with the hypogene gypsum karst of the Sant Miquel de Campmajor Valley, NE Spain. Geomorphology 328, 57–78.

Gutiérrez, F., Sevil, J., Migoń, P., 2023. Landslides in the Remolinos gypsum escarpment (NE Spain): controls imposed by stratigraphy, fluvial erosion, and interstratal salt dissolution. Landslides 20 (10), 2075–2093.

Gutiérrez, F., Deirnik, H., Zarei, M., Medialdea, A., 2023a. Geology, geomorphology and geochronology of the coseismic? Emad Deh rock avalanche associated with a growing anticline and a rising salt diapir, Zagros Mountains. Iran. Geomorphology 421, 108527.

Gutiérrez, F., Zarei, M., Hudec, M.R., Deirnik, H., 2023b. Normal faulting and landsliding in morpho-structural domes related to buried salt stocks, Zagros Mountains, Iran. Insights into salt breakout. Mar. Pet. Geol. 155, 106376.

Gutiérrez, F., Ilyati, I., Rezaei, M., Zarei, M., Hudec, M., 2024. Active strike-slip faulting, diapirism and seismic hazards. The case of the Kareh Bas fault and the associated Dandenjan salt extrusion in the Zagros Mountains, SW Iran. J. Struct. Geol. 187, 105239.

Gutiérrez, F., Zabramawi, Y., Memesh, A., Youssef, A.M., Bahamil, A., Auqué, L., 2025a. The geomorphology of monoclinal scarps associated with interstratal-dissolution fronts in evaporite formations, illustrated with the Upper Jurassic Arab and Hith formations in Ar Riyadh and Central Saudi Arabia. Earth-Sci. Rev. 261, 105032.

Gutiérrez, F., Haghighi, M.H., Ilyati, I., Motagh, M., del Val, M., 2025b. Diapiric and tectonic geomorphology of the river-damming Jahani salt extrusion associated with the strike-slip Kareh Bas fault, including DInSAR displacement data (Zagros Mountains, Iran). Geomorphology submitted.

Harrison, J.V., 1930. The geology of some salt-plugs in Laristan, southern Persia. Q. J. Geol. Soc. 86, 463–522.

Hassanpour, J., Jahani, S., Ghassemi, M.R., Alavi, S.A., Zeinali, F., 2018. Evolution of the Karebas Fault System and adjancent folds, central Zagros fold-and-thrust belt, Iran: Role of pre-existing halokinesis (salt structures and minibasins) and detachment levels. J. Asian Earth Sci. 164, 125–142.

Hessami, K., Koyi, H.A., Talbot, C.J., Tabasi, H., Shabanian, E., 2001a. Progressive unconformities within an evolving foreland fold–thrust belt, Zagros Mountains. J. Geol. Soc. Lond. 158, 969–981.

Hessami, K., Koyi, H.A., Talbot, C.J., 2001b. The significance of strike-slip faulting in the basement of the Zagros fold and thrust belt. J. Pet. Geol. 24, 5–28.

Hudec, M.R., Jackson, M.P.A., 2007. Terra infirma: understanding salt tectonics. Earth-Sci. Rev. 82 (1–2), 1–28.

Jahani, S., Callot, J.P., Frizon de Lamotte, D., Letouzey, J., Leturmy, P., 2007. The salt diapirs of the eastern Fars Province (Zagros, Iran): A brief outline of their past and present. In: Lacombe, O., Roure, F., Lavé, J., Vegés, J. (Eds.), Thrust Belts and Foreland Basins. Springer, Berlin, pp. 289–308.

Jahani, S., Callot, J.P., Letouzey, J., Frizon de Lamotte, D., 2009. The eastern termination of the Zagros Fold-and-Thrust Belt, Iran: structures, evolution, and relationships between salt plugs, folding, and faulting. Tectonics 28, TC6004.
Jahani, S., Hassanpour, J., Mohammadi-Firouz, S., Letouzey, J., de Lamotte, D.F., Alavi, S.A., Soleimany, B., 2017. Salt tectonics and tear faulting in the central part of the Zagros Fold-Thrust Belt, Iran. Mar. Pet. Geol. 86, 426–446.
Kent, P.E., 1958. Recent studies of south Persian salt plugs. AAPG Bull. 42 (12), 2951–2972.
Kent, P.E., 1979. The emergent Hormuz salt plugs of southern Iran. J. Pet. Geol. 2, 117–144.
Mann, P., Hempton, M.R., Bradley, D.C., Burke, K., 1983. Development of pull-apart basins. J. Geol. 91, 529–554.
Mehdizadeh, R., Zarei, M., Raeisi, E., 2015. How subaerial salt extrusions influnce wáter quality in adjacent aquifers. J. Hydrol. 531, 1108–1113.
Mouthereau, F., Tensi, J., Bellahsen, N., Lacombe, O., De Boisgrollier, T., Kargar, S., 2007. Tertiary sequence of deformation in a thin-skinned/thick-skinned collision belt: the Zagros Folded Belt (Fars, Iran). Tectonics 26, TC5006.
Naderi, M., Raeisi, E., Zarei, M., 2016. The impact of halite dissolution of salt diapirs on surface and groundwater under climate change, South-Central Iran. Environ. Earth Sci. 75, 708.
Nezamzadeh, I., Faghih, A., Oveisi, B., Kusky, T., Khajavi, N., Soleimani, M., Meng, J., 2024. On the use of displaced river terraces to characterize active tectonics of the Zagros orogenic belt, SW Iran. Results Earth Sci. 2, 100045.
Oveisi, B., Lavé, J., van der Beek, P., Carcaillet, J., Benedetti, L., Aubourg, C., 2009. Thick- and thin-skinned deformation rates in the central Zagros simple folded zone (Iran) indicated by displacement of geomorphic surfaces. Geophys. J. Int. 176, 627–654.
Palmer, A.N., 2007. Cave geology. Cave Books, Dayton, Ohio.
Pérez-Villar, G., Gutiérrez, F., Bausilio, G., Di Martire, D., 2025. Integrating DInSAR and detailed mapping for characterizing ground displacement in the Cardona salt extrusion related to diapiric uplift, disolutional lowering, landsliding and sinkholes. Eng. Geol. 352, 108068.
Phillips, J.D., 2017. Landform transitions in a fluviokarst landscape. Z. Geomorphol. 61, 109–122.
Phillips, J.D., Martin, L.L., Nordberg, V.G., Andrews Jr., W.A., 2004. Divergent evolution in fluviokarst landscapes of Central Kentucky. Earth Surf. Process. Landf. 29, 799–819.
Ruh, J.B., Hirt, A.M., Burg, J.P., Mohammadi, A., 2014. Forward propagation of the Zagros simply Folded Belt constrained from magnetostratigraphy of growth strata. Tectonics 33, 1534–1551.
Sevil, J., Gutiérrez, F., 2023. Morphometry and evolution of sinkholes on the western shore of the Dead Sea. Implications for susceptibility assessment. Geomorphology 434, 108732.
Shami, S., Shahriari, M.A., Nilfouroushan, F., Forghani, N., Salimi, M., Reshadi, M.A.M., 2024. Surface displacement measurement and modeling of the Shah-Gheyb salt dome in southern Iran using InSAR and machine learning techniques. Int. J. Appl. Earth Obs. Geoinf. 132, 104016.
Sherkati, S., Letouzey, J., Frizon de Lamotte, D., 2006. Central Zagros fold-thrust belt (Iran): New insights from seismic data, field observation, and sandbox modeling. Tectonics 25, TC4007.
Snidero, M., Muñoz, J.A., Carrera, N., Butillé, M., Mencos, J., Motamedi, H., Piryaei, A., Sàbat, F., 2019. Temporal evolution of the Darmadan salt diapir, eastern Fars region, Iran. Tectonophysics 766, 115–130.
Tackie-Otoo, B.N., Haq, M.B., 2024. A comprehensive review on geo-storage of H2 in salt caverns: Prospect and research advances. Fuel 356, 129609.
Taheri, K., Gutiérrez, F., Mohseni, H., Raeisi, E., Taheri, M., 2015. Sinkhole susceptibility mapping using the analytical hierarchy process (AHP) and magnitude-frequency relationships: a case study in Hamedan province. Iran. Geomorphology 234, 64–79.
Talbot, C.J., 1979. Fold trains in a glacier of salt in southern Iran. J. Struct. Geol. 1 (1), 5–18.
Talbot, C.J., Alavi, M., 1996. The past of a future syntaxis across the Zagros. Geol. Soc. Lond. Spec. Publ. 100, 89–109.
Talbot, C.J., Jarvis, R.J., 1984a. Age, budget and dynamics of an active salt extrusion in Iran. J. Struct. Geol. 6, 521–533.
Talbot, C.J., Jarvis, R.J., 1984b. Age, budget and dynamics of an active salt extrusion in Iran. J. Struct. Geol. 6, 521–533.
Talbot, C.J., Pohjola, V., 2009. Subaerial salt extrusions in Iran as analogues of ice sheets, streams and glaciers. Earth Sci. Rev. 97, 155–183.
Talbot, C.J., Medvedev, S., Alavi, M., Shahrivar, H., Heidari, E., 2000. Salt extrusion at Kuh-e-Jahani, Iran, from June 1994 to November 1997. Geol. Soc. Lond. Spec. Publ. 174, 93–110.
Tavakoli, F., Walpersdorf, A., Authemayou, C., Nankali, H.R., Hatzfeld, D., Tatar, M., Djamour, Y., Nilforoushan, F., Cotte, N., 2008. Distribution of the right-lateral strike–slip motion from the Main recent Fault to the Kazerun Fault System (Zagros, Iran): evidence from present-day GPS velocities. Earth Planet. Sci. Lett. 275, 342–347.
Tayebi, M.H., Tangestani, M.H., Roosta, H., 2013. Mapping salt diapirs and salt diapir-affected areas using MLP neural network model and ASTER data. Int. J. Digit. Earth 6 (2), 143–157.
Vernant, P., Nilforoushan, F., Hatzfeld, D., Abbassi, M.R., Vigny, C., Masson, F., Nankali, H., Martinod, J., Ashtiani, A., Bayer, R., Tavakoli, F., Chéry, J., 2004. Present-day crustal deformation and plate kinematics in the Middle East constrained by GPS measurements in Iran and northern Oman. Geophys. J. Int. 157, 381–398.
Walpersdorf, A., Hatzfeld, D., Nankali, H., Tavakoli, F., Nilforoushan, F., Tatar, M., Vernant, P., Chéry, J., Masson, F., 2006. Difference in the GPS deformation pattern of North and Central Zagros (Iran). Geophys. J. Int. 167, 1077–1088.
Wessel, B., 2016. TanDEM-X Ground Segment – DEM Products Specification Document. EOC, DLR, Oberpfaffenhofen, Germany, Public Document TD-GS-PS-0021, issue 3.2, 2016. [Online]. Available: https://tandemx-science.dlr.de/.
Williams, P.W., 1972. Morphometric analysis of polygonal karst in New Guinea. Geol. Soc. Am. Bull. 83, 761–796.
Williams, P.W., 2011. Karst in UNESCO World Heritage Sites. In: van Beynen, P.E. (Ed.), Karst Management. Springer, Dordrecht, pp. 459–480.
Zarei, M., 2016. Factors governing the impact of emerged salt diapirs on water resources. Groundwater 54, 354–362.
Zarei, M., Raeisi, E., 2010. Karst development and hydrogeology of Konarsiah salt diapir, south of Iran. Carbonates Evaporites 25, 217–229.
Zarei, M., Raeisi, E., Talbot, C., 2012. Karst development on a mobile substrate: Konarsiah salt extrusion. Iran. Geol. Mag. 149, 412–422.
Zhang, S., Jiang, Q., Shi, C., Xu, X., Gong, Y., Xi, J., Liu, W., Liu, B., 2021. Application of Sentinel-1 and-2 Images in measuring the Deformation of Kuh-e-Namak (Dashti) Namakier. Iran. Remote Sens. 13 (4), 785.